Reshaping the Primary Cell Wall: Dual Effects on Plant Resistance to Ralstonia solanacearum and Heat Stress Response

Henri Desaint, Alessandro Gigli, Adrien Belny, Hua Cassan-Wang, Yves Martinez, Fabienne Vailleau, Fabien Mounet, Samantha Verhnettes, Richard Berthome, Marta Marchetti

MPMI Vol. 37, No. 8, 2024, pp. 619–634, https://doi.org/10.1094/MPMI-05-24-0059-R

Reshaping the Primary Cell Wall: Dual Effects on Plant Resistance to *Ralstonia solanacearum* and Heat Stress Response

Henri Desaint,[1,2] Alessandro Gigli,[1,3] Adrien Belny,[1] Hua Cassan-Wang,[4] Yves Martinez,[5] Fabienne Vailleau,[1] Fabien Mounet,[4] Samantha Vernhettes,[6] Richard Berthomé,[1] and Marta Marchetti[1,†]

[1] Laboratoire des Interactions Plantes-Microbes-Environnement (LIPME), Université de Toulouse, INRAE, CNRS, Castanet-Tolosan 31320, France
[2] SYNGENTA Seeds, Sarrians 84260, France
[3] Department of Biology, University of Florence, Sesto Fiorentino, Italy
[4] Laboratoire de Recherche en Sciences Végétales, Université de Toulouse III, CNRS, INP, UMR5546, Castanet-Tolosan 31320, France
[5] Plateforme Imagerie, FRAIB-CNRS, Castanet-Tolosan 31320, France
[6] AgroParisTech, Institut Jean-Pierre Bourgin (IJPB), Université Paris-Saclay, INRAE, Versailles 78000, France

Accepted for publication 16 June 2024.

Temperature elevation drastically affects plant defense responses to *Ralstonia solanacearum* and inhibits the major source of resistance in *Arabidopsis thaliana*, which is mediated by the receptor pair RRS1-R/RPS4. In this study, we refined a previous genome-wide association (GWA) mapping analysis by using a local score approach and detected the primary cell wall *CESA3* gene as a major gene involved in plant response to *R. solanacearum* at both 27°C and an elevated temperature, 30°C. We functionally validated *CESA3* as a susceptibility gene involved in resistance to *R. solanacearum* at both 27 and 30°C through a reverse genetic approach. We provide evidence that the *cesa3^{mre1}* mutant enhances resistance to bacterial disease and that resistance is associated with an alteration of root cell morphology conserved at elevated temperatures. However, even by forcing the entry of the bacterium to bypass the primary cell wall barrier, the *cesa3^{mre1}* mutant still showed enhanced resistance to *R. solanacearum* with delayed onset of bacterial wilt symptoms. We demonstrated that the *cesa3^{mre1}* mutant had constitutive expression of the defense-related gene *VSP1*, which is upregulated at elevated temperatures, and that during infection, its expression level is maintained higher than in the wild-type Col-0. In conclusion, this study reveals that alteration of the primary cell wall by mutating the cellulose synthase subunit CESA3 contributes to enhanced resistance to *R. solanacearum*, remaining effective under heat stress. We expect that these results will help to identify robust genetic sources of resistance to *R. solanacearum* in the context of global warming.

†Corresponding author: M. Marchetti; Marta.Marchetti@inrae.fr

R. Berthomé and M. Marchetti contributed equally.

Funding: Support was provided by the FR-AIB Federation (AWARE project), Saclay Plant Sciences-SPS (ANR-17-EUR_0007), the Laboratoires d'Excellence (LABEX) TULIP (ANR-10-537-LABX-41), and the École Universitaire de Recherche (EUR) TULIP-GS (ANR-18-EURE-0019).

e-Xtra: Supplementary material is available online.

The author(s) declare no conflict of interest.

Keywords: *Arabidopsis thaliana*, cell wall, *CESA3*, *Ralstonia solanacearum*, temperature elevation

Plants are restricted to a sessile lifestyle and therefore must constantly cope with a fluctuating environment. In nature, they deal simultaneously with abiotic stresses (e.g., cold, heat, drought, salinity, flooding, and nutrient deficiency) and biotic stresses (e.g., pathogen infection and predation by herbivorous insects), both of which are major limitations affecting the distribution of wild plant species and crop yield (Saijo and Loo 2020). While the impact of climate change has been predicted for several decades (Bebber et al. 2013; IPCC 2022), the intensification of challenging environmental conditions will have increasingly obvious impacts on epidemics and global agricultural production (Desaint et al. 2021; Fleischer et al. 2017; Lobell et al. 2011; Moat et al. 2019; Rosenzweig et al. 2014).

In response to pathogens, plants have evolved a plethora of resistance mechanisms, which are either constitutively expressed or induced after pathogen attack (Couto and Zipfel 2016; Ding et al. 2022; Panstruga and Dodds 2009). One common resistance mechanism to all plant cells is the presence of a cell wall (CW) that often shields plants from pathogen invasion. CWs, both primary (P-CW) and secondary (S-CW) CWs, are complex composites mainly made of polysaccharides (i.e., cellulose, hemicellulose, and pectins), proteins, and lignin that is only present in the S-CW where it provides structural rigidity and hydrophobicity. They form complex, dynamic, and strong CW matrices (Höfte and Voxeur 2017). Modifications of CW composition and structure take place during plant development but also as a consequence of exposure to environmental stresses (e.g., abiotic stress or pathogen attack). These modifications impact cell wall integrity (CWI) and can initiate molecular adaptive mechanisms, such as CW composition remodeling and activation of defensive responses (Bacete et al. 2018, 2020; Vaahtera et al. 2019; Wolf et al. 2012). The mechanisms underlying CWI perception involves various plasma membrane receptors and complex signal transduction pathways, which help the plant to maintain its growth through development as well as to manage different adverse abiotic and biotic stresses (Swaminathan et al. 2022).

Particularly, in response to pathogens, defense mechanisms involve a diverse set of plasma membrane-resident pattern recognition receptors (PRRs) to detect damage-associated molecular patterns (DAMPs), 'nonself'-microbe-associated molecular patterns (MAMPs), or herbivore-associated molecular patterns (HAMPs) to activate pattern-triggered immunity (PTI). A sequence of events is activated in the cells, which includes signaling relays of defense-related genes, CW reinforcement, generation of antimicrobial secondary metabolites, and activation of the ethylene (ET), salicylic acid (SA), and jasmonic acid (JA) hormone pathways.

In terms of CWI and pathogen defense, the CrRLK1L receptor THESEUS1 (THE1), member of the RLK (receptor-like kinase) receptor subfamily, has been shown to be involved in the CWI-related signaling pathway, leading to callose induction, lignin synthesis, homogalacturonan enrichment, and the involvement of JA, ET, and SA hormones (Bacete et al. 2018; Gonneau et al. 2018).

Apart from THE1, another RLK, FERONIA (FER), is the most-widely studied receptor as a surface regulator and potential CW sensor (Ji et al. 2020). *Arabidopsis fer* mutants are resistant to the biotrophic fungus *Golovinomyces orontii* that causes powdery mildew, implying that FER negatively regulates plant immunity (Stegmann et al. 2017). In the *fer* mutants, the *PLANT DEFENSIN 1.2* (*PDF1.2*) marker gene transcript is induced by pathogens, demonstrating that FER is involved in ET- and JA-mediated defense pathways (Kessler et al. 2010).

Pathogen infection can induce CW degradation, releasing wall polysaccharides derived from homogalacturonans and cellulose (Lorrai and Ferrari 2021; Rui and Dinneny 2020). Treatments with cellulose-derived DAMPs (disaccharides to heptasaccharides) result in the activation of PTI (Pastor et al. 2022). Moreover, alteration of cellulose biosynthesis activates defense-signaling pathways, indicating that cellulose structure and composition are important parameters of plant CWI (Hamann 2012; Polko and Kieber 2019).

Cellulose is the main load-bearing component of both P-CW and S-CW conferring strength to plant cells (Höfte and Voxeur 2017). It is synthesized at the plasma membrane by the catalytic subunits of the cellulose synthase (CESA) protein complex (CSC). The P-CW CSC is exclusively composed of the isoforms CESA1, CESA3, and one of the CESA6-like isoforms such as CESA6, CESA5, CESA2, or CESA9 (Desprez et al. 2007; Persson et al. 2007), whereas the CSC in the S-CW involves CESA4, CESA7, and CESA8 (Atanassov et al. 2009). Altering expression or mutating the *CESA* genes has a specific impact on CWI and results in the release of DAMPs and activation of immune signaling, leading to either pathogen susceptibility or resistance (Bacete et al. 2018). *Arabidopsis thaliana irregular xylem* (*irx*) *5/3/1* CW mutants, which are defective in CESA 4/7/8 subunits required for S-CW formation, display enhanced resistance to several pathogens, including the necrotrophic fungi *Plectosphaerella cucumerina* and *Botrytis cinerea*, the vascular bacterium *Ralstonia solanacearum*, and the vascular fungus *Fusarium oxysporum* (Hernández-Blanco et al. 2007; Ramírez et al. 2011; Sánchez-Vallet et al. 2012; Swaminathan et al. 2022). This resistance relied on constitutive activation of plant immune responses, which is mainly accounted for by the abscisic acid (ABA)-responsive signaling pathway. Impairment of ABA signaling in the *Arabidopsis* ABA-deficient mutant *aba1-6* resulted in reduced cellulose and increased uronic acid in its CW, further resulting in resistance to *P. cucumerina* (Sánchez-Vallet et al. 2012). Similarly, mutating an *Arabidopsis* MYB46 transcription factor that regulates the expression of *CESA4/7/8* resulted in enhanced resistance to *B. cinerea* (Ramírez et al. 2011). In this case, the enhanced resistance to the fungus was due to heightened activation of the JA-regulated *PDF1.2* gene and genes encoding peroxidases. Furthermore, the *constitutive expression of the vegetative storage protein1* (*VSP1*) mutant (*cesA3*^{cev1}), showing constitutive activation of ET- and JA-related signaling genes, was more resistant to fungal pathogens and the bacterial pathogen *Pseudomonas syringae* (Ellis and Turner 2001; Ellis et al. 2002a). Altered cellulose synthesis also leads to changes in the response to abiotic stresses. For example, disruption of *Arabidopsis* S-CW by inactivation of the *CESA8/IRX1* gene in the *leaf wilting2* (*lew2*)*/irx1* mutant causes an increase in endogenous ABA levels and enhanced tolerance to drought and osmotic stress (Chen et al. 2005). Much less information is available on the role of the CW in conditions of heat stress. Temperature has been shown to influence the orientation of cellulose microfibrils and cellulose crystallinity, with the latter decreasing with heat (Fujita et al. 2011). However, to date, the contribution of the CW in responsiveness to a pathogen under elevated temperatures has not been established.

Genome-wide association (GWA) studies have provided insights into *A. thaliana* responses to *R. solanacearum* under heat stress (Aoun et al. 2017). In this latest study, a GWA study was conducted using a worldwide collection of *A. thaliana* wild accessions inoculated with *R. solanacearum* and cultivated either at 27°C or under heat stress at 30°C, mimicking a permanent increase in average surface temperature (of about 3°C). This study enabled the detection of quantitative trait loci (QTLs) underlying thermostable resistance mechanisms to the bacterium. Among them, *Strictosidine synthase-like protein 4* and *5* (*SSL4* and *SSL5*), as well as the atypical meiotic cyclin *SOLO DANCERS* genes, were functionally validated as susceptibility genes involved in quantitative disease resistance (QDR) to *R. solanacearum* at 30°C (Aoun et al. 2017, 2020). Another candidate gene identified at 30°C beneath these QTLs is *CESA3* (Aoun et al. 2017).

Here, we refined the GWA mapping analysis using the local score approach and identified the *CESA3* gene as playing a role in the plant response to *R. solanacearum* at both 27°C and under heat stress at 30°C (Bonhomme et al. 2019). Our study reveals that the *multiple response expansion 1* (*cesa3*^{mre1}) *A. thaliana* mutant enhances resistance against *R. solanacearum* at 27°C and maintains its increased resistance even under heat stress conditions (30°C). Expression analysis showed that the *cesa3*^{mre1} mutant constitutively expressed the JA-responsive genes *PDF1.2* and *VSP1*. In addition, *VSP1* expression was not only upregulated at elevated temperatures but also persisted higher than in susceptible genotypes upon *R. solanacearum* infection. These results indicate that alteration of plant P-CW composition and integrity can shield root bacterial entry and activate specific JA-mediated defensive pathways that could participate in plant-enhanced resistance responses while remaining efficient under elevated temperatures.

Results

The *CESA3* gene is a robust candidate involved in the response to *R. solanacearum* GMI1000

In a previous study, the genetic basis underlying plant responses to *R. solanacearum* at elevated temperatures was investigated in the worldwide *A. thaliana* collection using a GWA approach (Aoun et al. 2017). Upon bacterial infection and exposure to 30°C, one QTL was identified at the beginning of chromosome 5, with several top single nucleotide polymorphisms (SNPs) located at the *CESA3* locus (Aoun et al. 2017). The analysis of the linkage disequilibrium (LD) pattern under this QTL validated that *CESA3* was the most likely and unique candidate underlying this QTL (Aoun et al. 2017). We took advantage of a novel and more accurate post-GWA methodology (Bonhomme

et al. 2019) to calculate the local score on our previous GWA data (Aoun et al. 2017). With a tuning parameter of $\xi = 2$, the local score approach detected 54 and 71 unique QTLs at 27 and 30°C, respectively, analyzing all the time points of the kinetics (from day 3 to 11). We decided to focus on 38 QTLs (23 QTLs at 27°C, 12 QTLs at 30°C, and 3 QTLs common to both temperatures) that were the most significant, with a Lindley process value above 10, or which were highlighted at several days postinoculation (dpi) (Supplementary Table S1). Interestingly, among the three QTLs detected at both temperatures (QTL 3, 7, and 23), the most significant and highlighted for the most dpi was QTL 23, corresponding to the *CESA3* locus (Supplementary Table S1). Taking advantage of this method, we found that at 27°C, *CESA3* was detected at 9, 11, and 13 dpi with a Lindley process value just above 10, reaching 12.44 at 13 dpi (Fig. 1A to C). At 30°C, this QTL is present from 5 dpi, just above the significance threshold, to 7 dpi. It reaches its highest peak at 6 dpi, with a Lindley process value of 28.26 (Fig. 1D to F). No significant peak (Lindley process value above 10) corresponding to the *CESA3* locus could be detected at a time point earlier than 9 dpi at 27°C or later than 9 dpi at 30°C (Supplementary Fig. S1). These analyses point towards *CESA3* as a gene potentially involved in QDR to *R. solanacearum* at both temperatures. However, the temporality of its contribution to resistance is earlier at 30°C than at 27°C, with the most significant SNP found in *CESA3* (SNP–5–1530992) detected at 5 dpi at 30°C and only at 9 dpi at 27°C (Fig. 1).

The P-CW of the *cesa3^{mre1}* mutant results in enhanced resistance to *R. solanacearum* at both 27 and 30°C

Since the analysis of the local LD pattern validated *CESA3* as the most significant and common candidate locus underlying the quantitative plant response to *R. solanacearum* at both temperatures, we analyzed the impact of mutations in *CESA3* on the phenotypical response to the bacterium. At least nine different *cesa3* mutants have been identified so far in *A. thaliana* by ethyl methanesulphate (EMS) mutagenesis (Pysh et al. 2012). Among the *A. thaliana cesa3* mutants available, the previously described *isoxaben- resistant 1-1* mutant (*cesa3^{ixr1-1}*) is as susceptible as wild-type plants to *R. solanacearum* (Hernández-Blanco et al. 2007). Except for *cesa3^{ixr1-1}*, for which no obvious phenotypic differences from the wild-type are observed, most of the other *cesa3* mutants are affected constitutively in shoot development and root growth, showing a swelling root phenotype to varying degrees. Assuming that alteration of root tissue structure could impact *R. solanacearum* infection, we decided to test for infection with the root pathogen *R. solanacearum* in parallel to the *cesa3^{ixr1-1}* mutant, the *multiple response expansion 1* mutant, *cesa3^{mre1}* (also named *cesa3^{je5}*; Desprez et al. 2007), which, even if impacted in root development, has the least severe root phenotype among *cesa3* mutant lines (Pysh et al. 2012). Plants grown in jiffy pots were inoculated with *R. solanacearum* GMI1000, and the phenotypical response for the two mutants was monitored at 27 and 30°C and compared with the corresponding Col-0 wild-type accession. *cesa3^{ixr1-1}* was not only susceptible to *R. solanacearum*, as previously published, but statistical analysis based on the disease index (DI) score showed that it was even more susceptible than the wild-type Col-0 (Fig. 2A and B; Supplementary Fig. S2). Increased temperatures affected the kinetics of plant wilting for both Col-0 and *cesa3^{ixr1-1}*, with wilting symptoms appearing earlier at 30°C (2 dpi for *cesa3^{ixr1-1}* and 3 dpi for Col-0) compared with 27°C (4 dpi) and reaching complete wilting at 6 dpi at 30°C for both genotypes compared with 8 dpi for *cesa3^{ixr1-1}* or 10 dpi for Col-0 at 27°C (Fig. 2A and

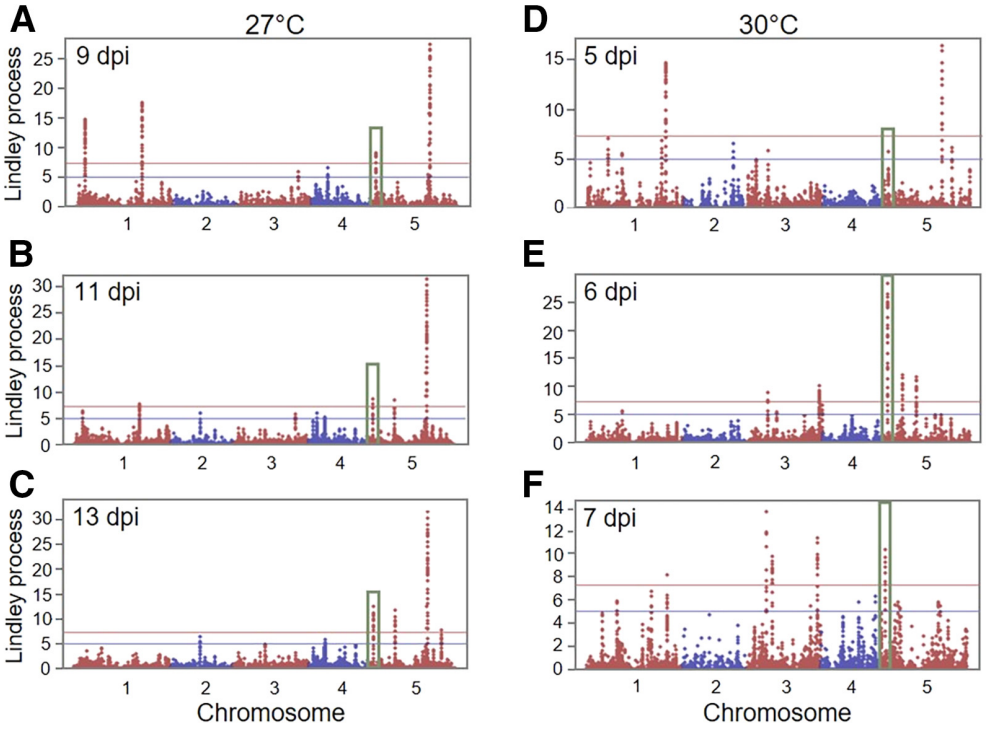

Fig. 1. The *CESA3* locus is detected at 27 and 30°C as conferring quantitative resistance to *Ralstonia solanacearum*. **A, B, and C,** Manhattan plot of the Lindley process (local score method with a tuning parameter of $\xi = 2$) at 9, 11, and 13 days postinoculation (dpi) for plants incubated at 27°C. **D, E, and F,** Manhattan plot of the Lindley process at 5, 6, and 7 dpi for plants incubated at 30°C. The green rectangle indicates the position of the quantitative trait locus (QTL) corresponding to the *CESA3* locus. The *y* axis corresponds to the Lindley process value, while the *x* axis corresponds to the physical position of the single nucleotide polymorphisms (SNPs) along the five chromosomes. The local score method was applied to the whole genome scan of 214,051 SNPs for association with the disease index at each selected day across the 163 accessions tested under combined inoculation and temperature treatment according to the method of Aoun et al. (2017). This method computes a significance threshold for each chromosome (*x* axis), where the blue horizontal line corresponds to the lowest threshold among the five chromosomes, and the red horizontal line corresponds to the highest threshold.

B). The faster onset of wilt symptoms observed in susceptible Col-0 and *cesa3*$^{ixr1\text{-}1}$ plants at 30°C may be attributed to enhanced virulence due to the optimal growth temperature of 30°C for *R. solanacearum* (Aoun et al. 2020; Wei et al. 2015). Interestingly, at both temperatures, the *cesa3*^{mre1} mutant not only showed a delay in disease symptom appearance but also remained significantly less susceptible than Col-0 and *cesa3*$^{ixr1\text{-}1}$ at all time points of the kinetics (Fig. 2A and B). At 7 (27°C) or 5 (30°C) dpi, the resistant phenotype of *cesa3*^{mre1} was macroscopically visible compared with wilted Col-0 and *cesa3*$^{ixr1\text{-}1}$ plants (Fig. 2C and D).

To determine whether the disease symptoms observed in *cesa3*^{mre1} correlated with reduced pathogen multiplication in planta, bacterial levels were measured in inoculated plants. Plants were collected at the appearance of the first symptoms of bacterial wilt in *cesa3*^{mre1} (mean of DI of 0.5). At 27°C, bacterial titers were significantly lower in *cesa3*^{mre1} compared with both Col-0 (mean DI of 1) and *cesa3*$^{ixr1\text{-}1}$ (mean DI of 2) (Fig. 2A and E). When exposed to 30°C, bacterial proliferation was still significantly lower for *cesa3*^{mre1} compared with Col-0 (average DI of 2.5) and *cesa3*$^{ixr1\text{-}1}$ (average DI of 3.5) (Fig. 2B and F).

Despite the well-documented severe impact of other *CESA3* mutations on root growth and development, we decided to analyze a third *cesa3* allele, the *ectopic lignification 1* (*cesa3*$^{eli1\text{-}1}$) mutant (Pysh et al. 2012; Supplementary Fig. S3A). As previously shown, the *cesa3*$^{eli1\text{-}1}$ mutant has significantly reduced shoot and root systems compared with the wild-type Col-0 (Caño-Delgado et al. 2003; Supplementary Fig. S3). Both Col-0 and *cesa3*$^{eli1\text{-}1}$ plants were inoculated with *R. solanacearum* and maintained at either 27 or 30°C. Remarkably, *cesa3*$^{eli1\text{-}1}$ plants exhibited significantly higher resistance compared with the wild-type Col-0 at both temperatures (Supplementary Fig. S3B and C). Although the potential influence of the strongly defective root phenotype on bacterial infection cannot be excluded for the *cesa3*$^{eli1\text{-}1}$ mutant, these findings support the hypothesis that CESA3 plays a pivotal role in enhancing resistance against *R. solanacearum*.

Altogether, these data indicate that CESA3 is important for *R. solanacearum* pathogenicity, acting as a susceptibility factor

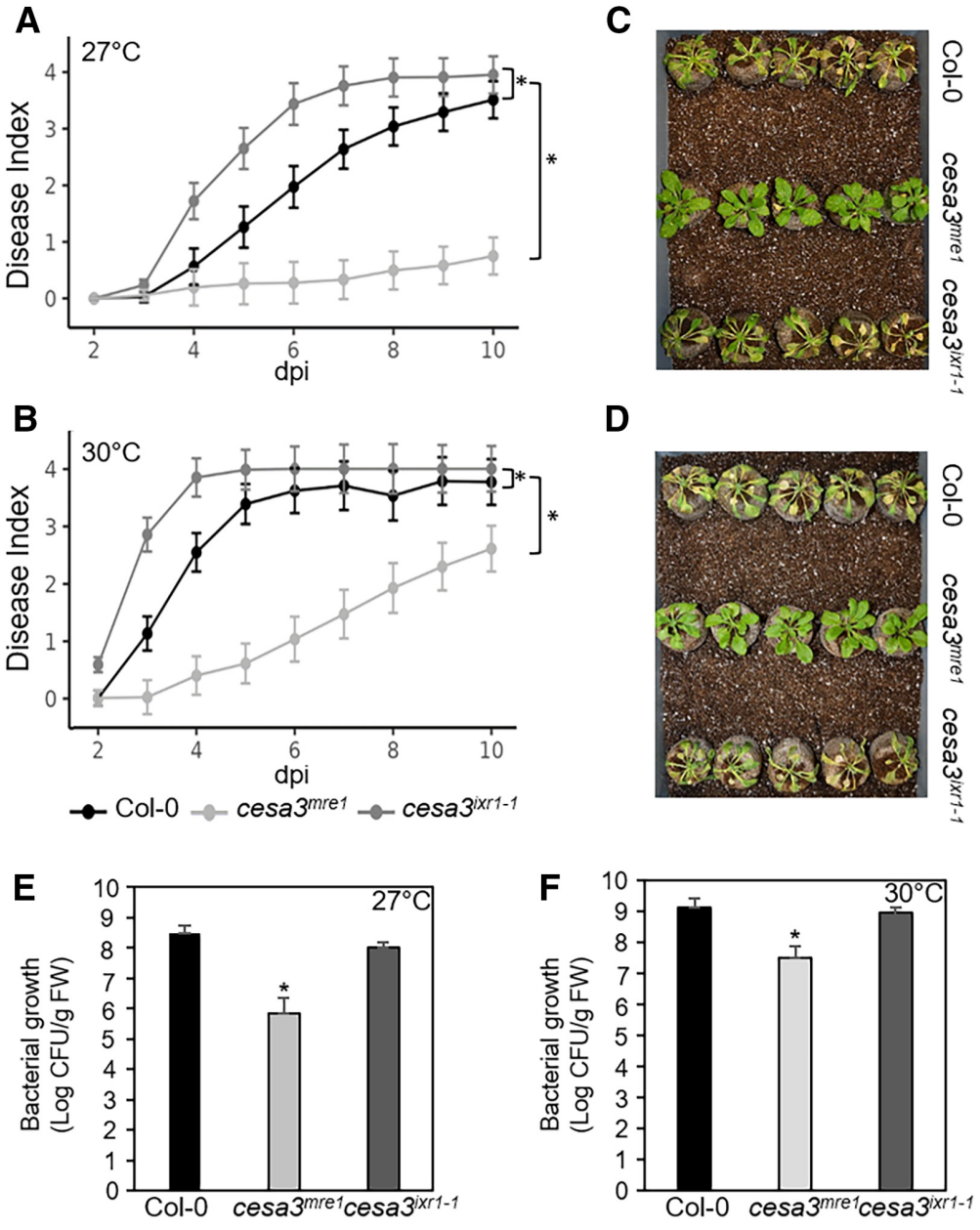

Fig. 2. The *Arabidopsis thaliana cesa3*^{mre1} mutant enhances resistance to *Ralstonia solanacearum* at both 27 and 30°C. Four-week-old plants of the wild-type (Col-0) and *cesa3* mutants (*cesa3*^{mre1} and *cesa3*$^{ixr1\text{-}1}$) were challenged with the *R. solanacearum* GMI1000 strain and monitored for disease symptoms appearance at **A,** 27°C and **B,** 30°C. Curves represent the least-square-means (lsmeans) ± standard errors of the lsmeans from three independent experiments conducted for each condition. Pairwise differences were calculated with the area under the disease curve (AUC) method. Significant differences are denoted with asterisks (*) ($P < 0.001$). **C and D,** Representative photographs of infected plants taken at 7 and 5 days postinoculation (dpi) at 27°C and 30°C, respectively. **E and F,** In planta growth of *R. solanacearum* GMI100 strain in wild-type and *cesa3* mutant plants exposed to 27 and 30°C and recovered at 5 and 4 dpi, respectively. Plants were inoculated using a root drenching method (1×10^8 colony-forming units [CFU])/ml). Bars represent the mean number ± standard errors of nine plants per genotype of each condition from two independent experiments. Significant differences are indicated with an asterisk (*) according to the *t* test ($P < 0.05$). FW, fresh weight.

that contributes to bacterial wilt establishment and functioning even under heat stress conditions.

The *cesa3^{mre1}*-mediated resistance to *R. solanacearum* correlates with altered root morphology

Mutations in *CESA3* in the *cesa3^{ixr1-1}* and *cesa3^{mre1}* genotypes are single nucleotide substitutions, leading to Gly998Asp and Gly916Glut amino acid changes located in the fifth and seventh transmembrane domains of the CESA3 protein, respectively, which could differently affect cellulose structure and CW composition (Pysh et al. 2012; Scheible et al. 2001; Supplementary Fig. S4). Fourier transformed infrared (FT-IR) fingerprinting spectroscopy showed a CW composition profile that allowed discrimination of *cesa3^{mre1}* compared with both *cesa3^{ixr1-1}* and Col-0, which show an almost identical spectrum (Supplementary Fig. S5; Supplementary Table S2). Indeed, when grown in vitro at the permissive temperature (22°C), the two mutants displayed clearly different root phenotypes. In agreement with previous observations, *cesa3^{mre1}* shows shorter and enlarged roots compared with those of *cesa3^{ixr1-1}*, which behaved similarly to the wild-type Col-0 (Pysh et al. 2012; Scheible et al. 2001; Fig. 3A). When observed at 27 and 30°C, the root growth and macroscopic phenotype in *cesa3^{mre1}* appeared unaffected by temperature elevation and remained clearly different from *cesa3^{ixr1-1}* and Col-0 (Fig. 3B; Supplementary Fig. S6). To further visualize the effect of the *cesa3* mutations on root cell architecture, we made semithin sections of *cesa3^{mre1}* and *cesa3^{ixr1-1}* roots exposed to 22, 27, and 30°C and compared them to the Col-0 wild-type accession. After staining with Calcofluor, which is a nonspecific fluorochrome known to bind CW compounds, particularly cellulose, the fluorescent signal was observed to extensively distribute in the CW of all the analyzed sections (Fig. 4). Confocal observations revealed a strong difference in root cell size of *cesa3^{mre1}* when compared with Col-0 and *cesa3^{ixr1-1}* (Fig. 4; compared 22, 27, and 30°C). The rise in temperature had no discernible effect on root cell organization and morphology in the *cesa3^{mre1}* mutant, which consistently exhibited enlarged cortical cells across the three temperature conditions, differing from both the wild-type Col-0 and the *cesa3^{ixr1-1}* mutant (Fig. 4). A slight increase in cell size was noted for both Col-0 and *cesa3^{ixr1-1}* exposed to 30°C. However, it did not correlate with noticeable alterations in primary root morphology (Fig. 3B; Supplementary Fig. S6). Additionally, no obvious modifications were observed in the cellulose fluorescent signals upon exposure to increased temperatures for any of the genotypes analyzed. The c*esa3^{mre1}* mutant has been shown to have a lower cellulose content than Col-0 (Pysh et al. 2012). To further analyze whether temperature could impact CW composition, we determined cellulose content in roots of Col-0, *cesa3^{mre1}*, and *cesa3^{ixr1-1}* genotypes grown either at 27 or 30°C and compared them to those obtained at the permissive growth temperature (22°C). In all temperature conditions, the cellulose content in *cesa3^{mre1}* roots was reduced compared with Col-0 and *cesa3^{ixr1-1}* (Supplementary Fig. S7).

Root integrity in the *cesa3^{mre1}* mutant contributes to the resistance response to *R. solanacearum*

R. solanacearum is a soilborne pathogen that infects plants through the roots before reaching the xylem vessels and spreading within the plant. Given that *cesa3^{mre1}* exhibits an altered root phenotype characterized by short and swollen cells, the significant delay in disease onset and reduced symptoms observed may stem from difficulties encountered by the bacterium in penetrating the root tissues. To investigate this possibility, disease symptom appearance was monitored in Col-0 and *cesa3^{mre1}* plants at 27 or 30°C challenged with *R. solanacearum* after root wounding by cutting the bottom of each jiffy pot to provide the bacteria with direct access to the xylem vessels. As expected, root cutting rendered Col-0 plants more susceptible, with disease symptoms appearing at least 1 day earlier postinfection at both 27 and 30°C compared with uncut conditions (Figs. 2A and B and 5A). Root cutting also significantly impacted the disease resistance of *cesa3^{mre1}*. Notably, at both temperatures, the disease progression dynamics in *cesa3^{mre1}* plants resembled those in Col-0 (Fig. 5A), indicating that allowing bacteria to have direct access to the xylem strongly influences the "resistant pattern" conferred by the *cesa3^{mre1}* mutation. However, *cesa3^{mre1}* remained statistically less susceptible than Col-0 at 27°C (Fig. 5A), whereas at 30°C, a significant difference between the wild-type and the mutant was observed only at the early stages of the infection process (Fig. 5A; Supplementary Fig. S8). Specifically, the onset of symptoms in Col-0 at both temperatures occurred on average 1.8 days earlier than in *cesa3^{mre}* (Fig. 5A; Supplementary Fig. S8). Bacterial colonization levels were assessed in infected plants at either 27 or 30°C, which were sampled upon the onset of the first wilt symptoms in *cesa3^{mre1}* (average DI of 0.5), corresponding

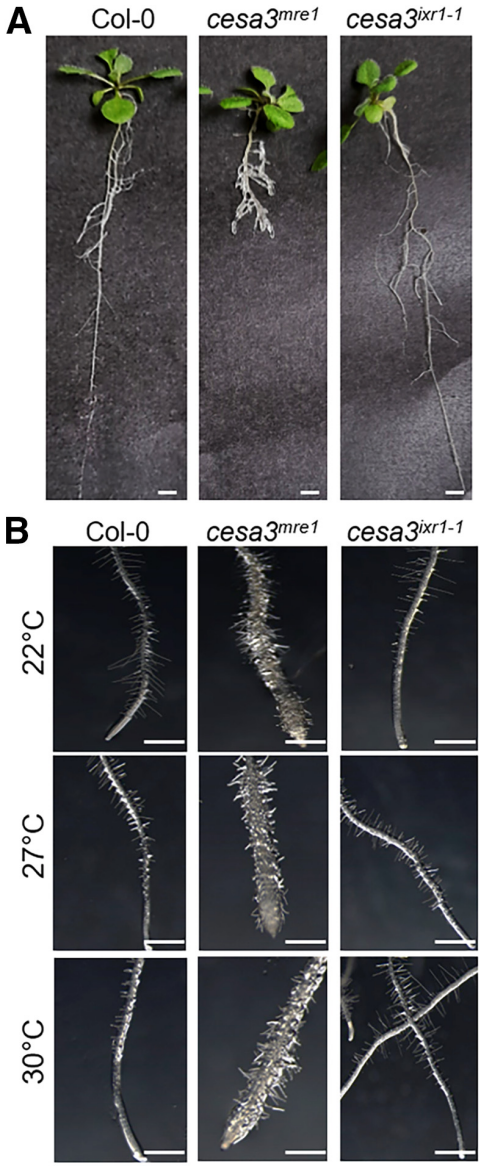

Fig. 3. The *cesa3^{mre1}* mutant is affected in plant growth and root phenotype. **A,** Seven-day-old seedlings of wild-type Col-0 and *cesa3* mutants were cultivated in vertical square plates for 10 days at 22°C. **B,** Detail of root tip growth of Col-0 and *cesa3* mutants grown at 22°C or placed for 5 days at 27 or 30°C. Scale bars represent 2 mm.

to DI values for Col-0 of 2 and 1, respectively. At both temperatures, bacterial multiplication in *cesa3*^{mre1} plants was significantly lower than in Col-0 plants (Fig. 5B). These findings collectively suggest that despite the bypassing of the modified P-CW physical barrier, the *cesa3*^{mre1} mutation is involved in the early establishment of a defense response at both 27 and 30°C.

Plant colonization progress is impaired in the *cesa3*^{mre1} mutant

Since root wounding reduced resistance to *R. solanacearum* in *cesa3*^{mre1}, the altered root phenotype observed in *cesa3*^{mre1} could mainly serve as a physical barrier against bacterial invasion. To investigate this aspect, we used an in vitro inoculation procedure of intact roots adapted from Digonnet et al. (2012) to compare the colonization capacity of *R. solanacearum* in *cesa3*^{mre1} roots with that in Col-0 and *cesa3*$^{ixr1\text{-}1}$. Consistent with the phenotyping in jiffy pots, albeit with varying kinetics, *cesa3*^{mre1} plants exhibited enhanced resistance to *R. solanacearum* (Fig. 6). Within 7 dpi, infected Col-0 and *cesa3*$^{ixr1\text{-}1}$ plants exposed to 30°C became chlorotic and displayed a wilting phenotype compared with the resistant *cesa3*^{mre1} infected plants (Fig. 6A). The same wilting phenotype could be observed at 10 dpi in Col-0 and *cesa3*$^{ixr1\text{-}1}$ placed at 27°C (data not shown). Plants inoculated with a GMI1000 strain constitutively expressing green fluorescent protein (GFP) (GMI1000 eGFP) were analyzed for bacterial colonization. This showed that the onset of disease symptoms correlated with bacterial progression in plant tissue. Notably, at 5 dpi at 30°C, bacterial progression could be observed in Col-0 and *cesa3*$^{ixr1\text{-}1}$ at the base of the rosette, which is a bottleneck in the *R. solanacearum* wilting process (Planas-Marquès et al. 2020). In contrast, no fluorescent bacteria could be detected in inoculated *cesa3*^{mre1} plants above the plantlets' collar (Fig. 6B).

To further characterize the presence of bacteria throughout root during infection, roots of inoculated plants were harvested at 2, 5, and 7 dpi at both temperatures and were used to quantify bacterial colonization (Fig. 6C).

At 2 dpi, infected roots showed a comparable number of colonizing bacteria for the three genotypes when exposed to 27°C. At 30°C, a higher number of colonizing bacteria were retrieved from the roots of all three genotypes. However, bacterial colonization was still significantly reduced in *cesa3*^{mre1} compared with Col-0 and *cesa3*$^{ixr1\text{-}1}$(Fig. 6C). The higher bacterial titers at 30°C during the early infection process likely reflect the ability of *R. solanacearum* cells to thrive better at higher temperatures, with 30°C being its optimal growth temperature (Aoun et al. 2020; Wei et al. 2015). At 5 and 7 dpi, in planta bacterial multiplication was still significantly reduced in *cesa3*^{mre1} at both 27 and 30°C compared with Col-0 and *cesa3*$^{ixr1\text{-}1}$ (Fig. 6C). At these time points, the impact of elevated temperatures on bacterial multiplication in roots was not observed to a greater extent for Col-0 and *cesa3*$^{ixr1\text{-}1}$, possibly because most bacteria had already reached the xylem vessels and that their multiplication rate within roots might be less sensitive to external temperature.

Altogether, these results suggest that in the *cesa3*^{mre1} mutant, alterations in the P-CW structure impede bacteria pene-

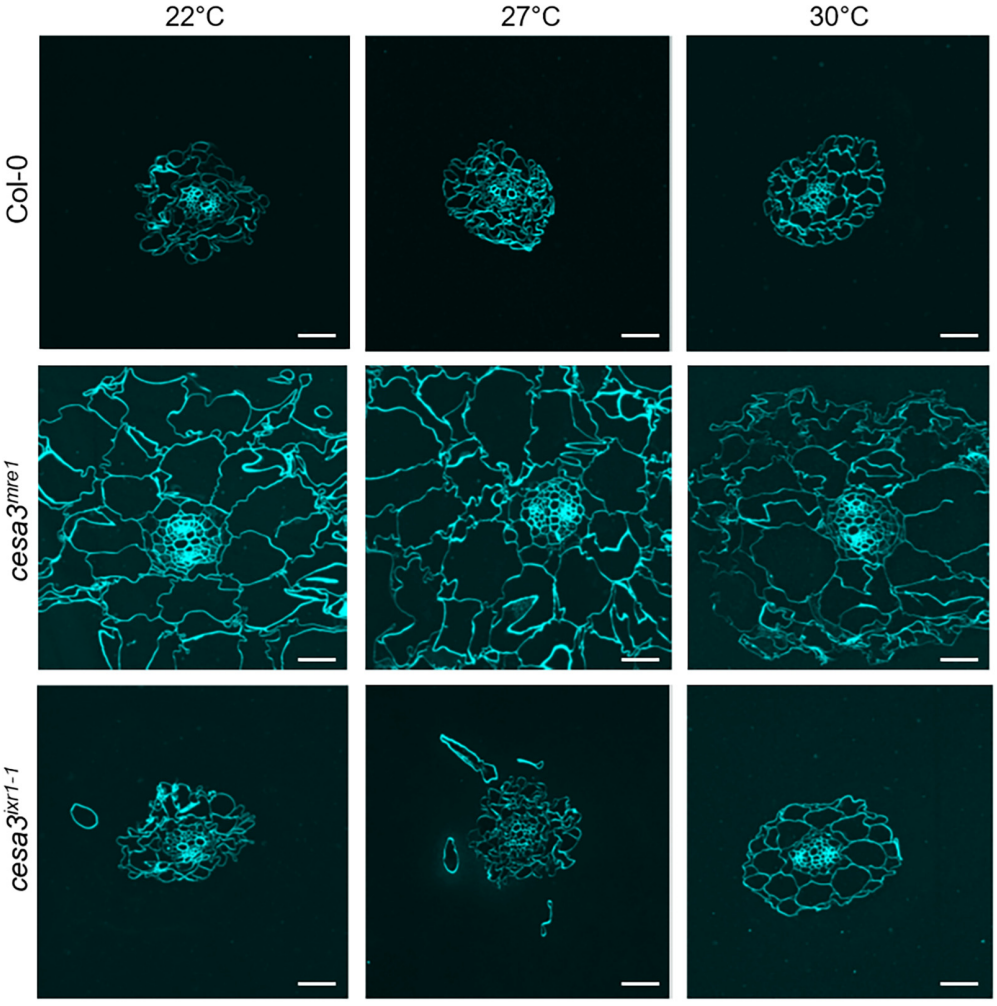

Fig. 4. The *cesa3*^{mre1} mutant exhibits enlarged cells independently of temperature. Semi-thin sections of 3-week-old plant roots grown using the in vitro square plate method were Calcofluor-stained, showing the organization of the cell layers of the roots for each genotype at different temperatures. Scale bars represent 20 μm.

tration into root tissue, thereby limiting colonization of xylem vessels.

The two other subunits of the P-CW cellulose synthase complex, CESA1 and CESA6, are also required for *R. solanacearum* pathogenicity

In *A. thaliana*, the P-CW is synthesized by a multiprotein complex involving CESA1, CESA3, CESA6, or CESA6-like proteins in a 1:1:1 stoichiometry (Gonneau et al. 2018; Hill et al. 2014). While only the *CESA3* gene was detected in the GWA mapping (Aoun et al. 2017), even after the use of the local score mapping approach (Bonhomme et al. 2019; this study), the functional proximity between these *CESA* genes prompted us to determine whether mutations in either *CESA1* or *CESA6* could modulate the plant response to *R. solanacearum* infection at both 27 and 30°C. We therefore used the *CESA1 radially swollen 1* (*cesa1*$^{rsw1\text{-}10}$) mutant and the null mutant *CESA6 PROCUSTE 1* (*cesa6*$^{prc1\text{-}1}$), with the mutations being in Ws-2 and Col-0 backgrounds, respectively (Arioli et al. 1998; Fagard et al. 2000). While both mutants display altered root growth phenotypes including stunted growth and thicker roots, owing to cellulose deficiency, the null *cesa6*$^{prc1\text{-}1}$ mutant exhibits milder phenotypes than *cesa1*$^{rsw1\text{-}10}$ (Fagard et al. 2000; Supplementary Fig. S9). Unlike Col-0, which is susceptible to *R. solanacearum* GMI1000 at both temperatures, Ws-2 is resistant at 27°C due to the presence of the RRS1-R/RPS4 NLR pair involved in PopP2 effector recognition (Deslandes et al. 2002). This immune receptor complex is functional at 27°C but not at 30°C (Aoun et al. 2017). Therefore, the response to *R. solanacearum* of *cesa1*$^{rsw1\text{-}10}$ was only followed at 30°C, as this mutation was obtained in the Ws-2 genetic background. The experiments were performed at 30 and 27°C for the *cesa6*$^{prc1\text{-}1}$ mutant, which was obtained in the Col-0 genetic background that is susceptible regardless of the temperature applied. At 27°C, the *cesa6*$^{prc1\text{-}1}$ mutant showed a very strong and significant decrease in wilting symptom appearance compared with Col-0, which correlates with a previous report (Menna et al. 2021; Fig. 7A). At 30°C, disease development was strongly and significantly decreased in both *cesa1*$^{rsw1\text{-}10}$ and *cesa6*$^{prc1\text{-}1}$ mutants at all time points after bacterial challenge when compared with their respective wild-type genotypes (Fig. 7A). Subsequently, we evaluated the in planta bacterial colonization of *R. solanacearum* by harvesting the rosette of infected plants when *cesa1*$^{rsw1\text{-}10}$ and *cesa6*$^{prc1\text{-}1}$ mutants showed a DI of approximately 0.5 as for *cesa3*^{mre1}. For both mutants, the decrease in wilting symptom development was accompanied by a significant decrease in pathogen content compared with their corresponding wild-type genotype when exposed to 27 and/or 30°C (Fig. 7B). When comparing the bacterial titers of the mutants at 27 and 30°C, we still observed the impact of temperature elevation on bacterial multiplication. However, this could not be observed for the wild-type genotype (Col-0 and Ws-2), possibly due to the deteriorating plant tissue of the plants having a high DI (around 3 to 3.5) (Fig. 7B). These results clearly highlight CESA1 and CESA6 as additional susceptibility factors that contribute to bacterial wilt establishment and bacterial colonization. Altogether, these data

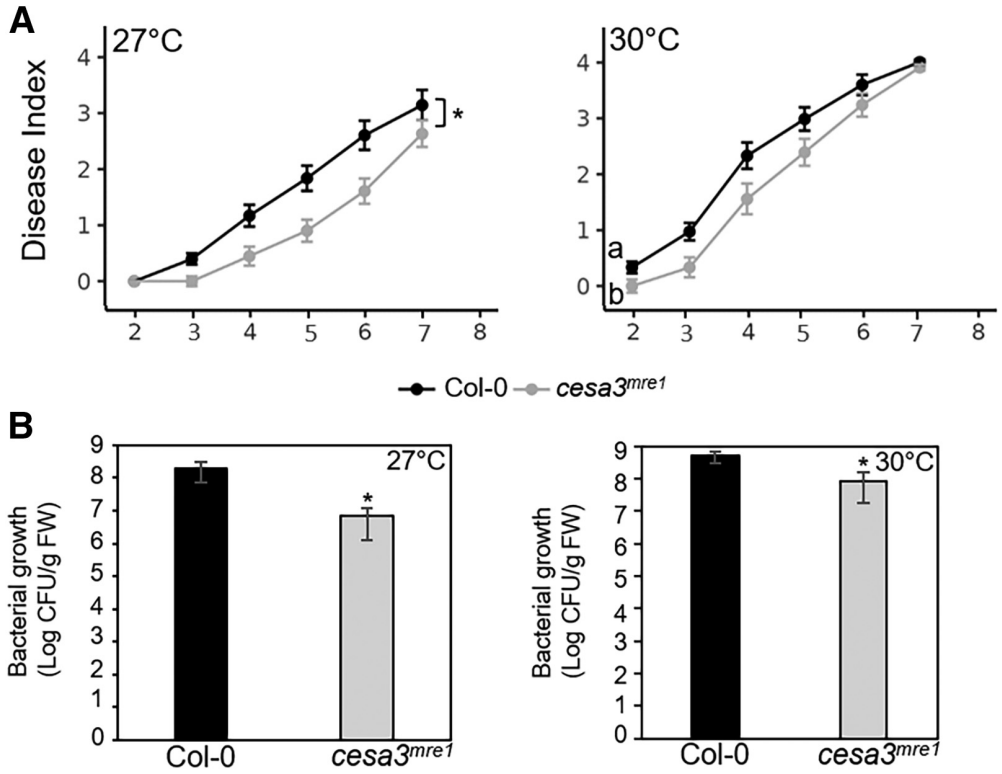

Fig. 5. Direct access to the xylem alters the susceptibility of the *Arabidopsis thaliana cesa3*^{mre1} mutant to *Ralstonia solanacearum*. **A,** Roots of 4-week-old Col-0 and *cesa3*^{mre1} plants growing in jiffy pots were cut before infection with *R. solanacearum* GMI1000 using the soil-drenching method. Disease symptom appearance was scored at both 27 and 30°C. Curves represent the least-square-means (lsmeans) ± standard errors of the lsmeans from three independent experiments. Pairwise differences were assessed by area under the disease curve (AUC) values and were used to compute lsmeans. Statistical significance is indicated by an asterisk (*), while "a" and "b" indicate statistical differences based on the day of appearance of the first symptoms ($P < 0.001$). **B,** In planta growth of *R. solanacearum* inoculated in Col-0 and *cesa3*^{mre1} in the root cut condition at 27 and 30°C and recovered at 5 and 3 days postinoculation (dpi), respectively. Three different plants were assessed per genotype for three independent experiments per condition. Values are means ± standard errors. Significant differences are indicated by asterisks (*) determined by a *t* test ($P < 0.05$). FW, fresh weight.

suggest that a functional CSC complex is required for full *R. solanacearum* pathogenicity at both 27 and 30°C.

Cell wall alteration in *cesa3*^{mre1} does not modify the expression of P-CW cellulose synthase complex subunits *CESA3*, *CESA1*, and *CESA6*

The difference between the two *CESA3* alleles *cesa3*^{mre1} and *cesa3*$^{ixr1\text{-}1}$ in root morphology and consequent susceptibility to *R. solanacearum* could be due to a differential expression profile of the *CESA3* gene. We used quantitative real-time PCR (RT-qPCR) to verify *CESA3* expression levels in *cesa3*^{mre1} and *cesa3*$^{ixr1\text{-}1}$ plantlets compared with Col-0. At 22°C, no significant difference was observed in *CESA3* gene expression between *cesa3*^{mre1}, *cesa3*$^{ixr1\text{-}1}$, and the wild-type Col-0 genotype (Supplementary Fig. S10). Similarly, we did not detect any differences in the expression levels of *CESA1* and *CESA6* between Col-0, *cesa3*^{mre1}, and *cesa3*$^{ixr1\text{-}1}$ (Supplementary Fig. S10). Exposure to elevated temperatures (27 and 30°C) did not induce significant differences in *CESA1*, *CESA3*, and *CESA6* gene expression in any of the three genotypes (Supplementary Fig. S10). These data suggest that the *cesa3*^{mre1} mutation does not affect the gene expression of the CSC subunits even under higher temperatures and that the root morphology in *cesa3*^{mre1} could be linked to an alteration of the function of CESA3.

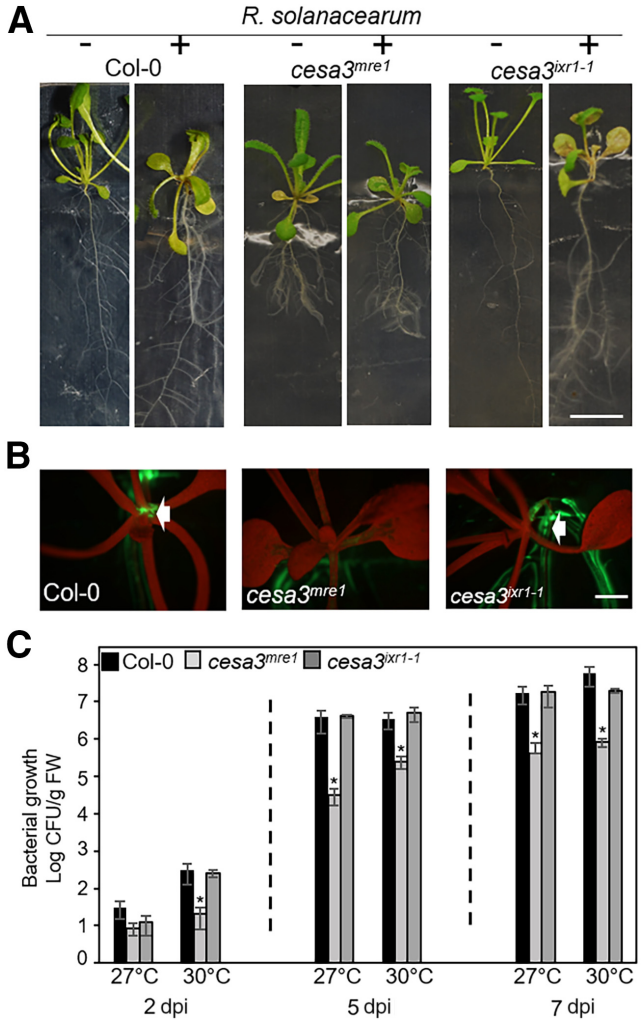

Fig. 6. Cell wall alterations in the *cesa3*^{mre1} mutant affect *Ralstonia solanacearum* root colonization. Seven-day-old seedlings of wild-type Col-0, *cesa3*^{mre1}, and *cesa3*$^{ixr1\text{-}1}$ were grown for 7 days in the vertical square plate in vitro system and then mock inoculated with water or inoculated with the *R. solanacearum* GMI1000 green fluorescent protein (GFP)-expressing strain. **A,** Photographs of plants placed at 30°C were taken at 7 days postinoculation (dpi) to show chlorosis and wilting symptoms in Col-0 and *cesa3*$^{ixr1\text{-}1}$. The scale bar represents 1 cm. **B**, At 5 dpi, bacterial progression could be observed at the base of the rosette for Col-0 and *cesa3*$^{ixr1\text{-}1}$ at 30°C. The scale bar represents 0.5 cm. **C,** *Arabidopsis thaliana* Col-0, *cesa3*^{mre1}, and *cesa3*$^{ixr1\text{-}1}$ were grown in vitro, and roots were recovered at 2, 5, and 7 dpi. Colony-forming units (CFU) per gram of roots was evaluated. Each bar represents the mean value ± standard errors (in log) for three independent experiments. For each experiment and genotype, three samples of three roots each were taken. Significant differences among the three genotypes for each temperature and time point are indicated by asterisks (*) according to the *t* test ($P < 0.05$). FW, fresh weight.

cesa3^{mre1} constitutively expresses JA- and ET-responsive genes *VSP1* and *PDF1.2* but not SA- or ABA-related signaling genes

Alterations in CW, including *cesa3* mutants, have been shown to correlate with altered constitutive expression of hormone-responsive genes (Ellis et al. 2002b) and to enhanced resistance against biotrophic and necrotrophic pathogens (Ellis and Turner 2001; Ellis et al. 2002a; Hernández-Blanco et al. 2007). To determine whether *cesa3*^{mre1} leads to misregulation of the expression of hormone-defense-signaling genes, 7-day-old plantlets growing at 22°C were collected to measure gene expression by RT-qPCR analysis. We found that transcripts of the JA- and ET-responsive genes *VSP1* and *PDF1.2* were upregulated in *cesa3*^{mre1} compared with Col-0 *and cesa3*$^{ixr1\text{-}1}$ plants (Fig. 8A and B). Previous studies showed that mutations of the *CESA* genes involved in S-CW formation (*CESA8*, *CESA7*, and *CESA4*) and constitutively expressing ABA-responsive genes conferred enhanced resistance to *R. solanacearum* (Hernández-Blanco et al. 2007). We then tested whether the expression of SA- and ABA-responsive genes were altered in the *cesa3*^{mre1} mutant. RT-qPCR analysis showed that expression of ABA- and SA-signaling genes, namely *ABI5* and *CBP60g*, respectively, was comparable in the two mutants and Col-0 (Fig. 8C and D).

Increasing temperature upregulates the expression of the JA-responsive gene *VSP1* in the *cesa3*^{mre1} mutant independently of bacterial infection

We examined whether temperature elevation or *R. solanacearum* infection could modulate the expression of JA- and ET-related genes. Plants were maintained at the permissive temperature (22°C) or exposed to 27 and 30°C, and gene expression was analyzed. We used the in vitro culture system to specifically monitor gene expression at the root level, the site of entry for the bacterium. The heat-inducible gene *HSP70* was used to check the induction of the heat stress response. As expected, *HSP70* expression was significantly upregulated with temperature elevation for all three genotypes, showing a higher level of expression in roots of control noninoculated plants exposed to 30°C (Fig. 9A). In roots of control plants, *PDF1.2* expression was rapidly impaired with temperature elevation (22 < 27 < 30°C) (Fig. 9B). This result correlates with the downregulation of *PDF1.2* triggered by temperature elevation, as previously reported (Huot et al. 2017). Notably, 5 days after exposure to elevated temperatures, gene expression was strongly downregulated for all the genotypes tested (Fig. 9B; panel 30°C). In contrast, the expression level of *VSP1* in *cesa3*^{mre1} was rapidly upregulated by temperature elevation, while it remained low and stable in Col-0 and the *cesa3*$^{ixr1\text{-}1}$ mutant 2 days after temperature exposure (Fig. 9C). Interestingly, bacterial infection led to a reduced expression level of *VSP1* in the *cesa3*^{mre1} genotype at both temperatures compared with uninfected control roots at 2 dpi. In contrast, infection enhanced *VSP1* gene expression in Col-0 and *cesa3*$^{ixr1\text{-}1}$. Nonetheless,

the *VSP1* expression level remained significantly higher in *cesa3*^{mre1} than in Col-0 and *cesa3*$^{ixr1\text{-}1}$.

Discussion

The P-CW *CESA3* gene was previously identified in a GWA mapping approach highlighting a specific QTL associated with the *A. thaliana* defense responsiveness to *R. solanacearum* under heat stress at 30°C (Aoun et al. 2017). Based on a more accurate method of analysis, we show, in this study, that this specific QTL is also detected at 27°C, the canonical temperature used for this pathosystem, making *CESA3* a strong candidate to be involved in the response to *R. solanacearum*. This raises the significant question of whether *CESA3* could be involved in plant defense against *R. solanacearum* as a susceptibility gene. Previous work by Hernández-Blanco et al. (2007) showed that a *cesa3* mutant, the *isoxaben-resistant 1-1* mutant *cesa3*$^{ixr1\text{-}1}$, was as susceptible as the wild-type Col-0 in response to *R. solanacearum* (Hernández-Blanco et al. 2007). To date, *cesa3*$^{ixr1\text{-}1}$ is one of the nine *cesa3* allelic mutants that have been identified by different approaches (Heim et al. 1989; Hu et al. 2016; Persson et al. 2007; Pysh et al. 2012; Sethaphong et al. 2013). Most of these mutants are strongly affected in shoot and root morphology as well as cellulose content (Pysh et al. 2012), and *cesa3*$^{ixr1\text{-}1}$ is the only mutant that does not have morphological abnormalities showing a wild-type phenotype (Turner and Somerville 1997; this study). Root morphology and CW structure are critical parameters that have been proposed to contribute to resistance to pathogens (Ishida and Noutoshi 2022; Planas-Marquès et al. 2020). To address this point, we studied another allelic mutant of *cesa3*, *the multiple response expansion1* mutant *cesa3*^{mre1}. Even though this mutant is still affected in root growth and morphology, its development allows infection with the root pathogen *R. solanacearum*. Contrary to *cesa3*$^{ixr1\text{-}1}$, we demonstrated that the *cesa3*^{mre1} mutant showed enhanced resistance to *R. solanacearum* at both temperatures, 27 and 30°C. We found that both mutants displayed comparable mRNA levels for *CESA3*, *CESA1*, and *CESA6*, suggesting that the distinct phenotype and response to *R. solanacearum* infection are due to the impact of the mutation on the protein function. Both mutations are localized in transmembrane domains of the CESA3 subunit, and even though a functional role has been demonstrated for the CESA transmembrane region, whether and how these mutations affect protein stability and CSC formation and function remains to be elucidated (Harris et al. 2012; Shim et al. 2018). The GWA mapping analysis showed different kinetics of appearance of the QTL associated with *CESA3*. We can speculate that the timing of establishment of the response to the pathogen involving the P-CW *CESA3* might depend on temperature, occurring earlier at 30 than 27°C. This correlates with the impact temperature elevation has on the timing of appearance of wilting symptoms in the susceptible wild-type Col-0 and *cesa3*$^{ixr1\text{-}1}$ plants, which was earlier at 30°C than at 27°C. Furthermore, the in vitro plant growth system showed that at the same dpi, a higher bacterial titer could be recovered from infected roots, particularly at the early time points of the infection process. This is in line with

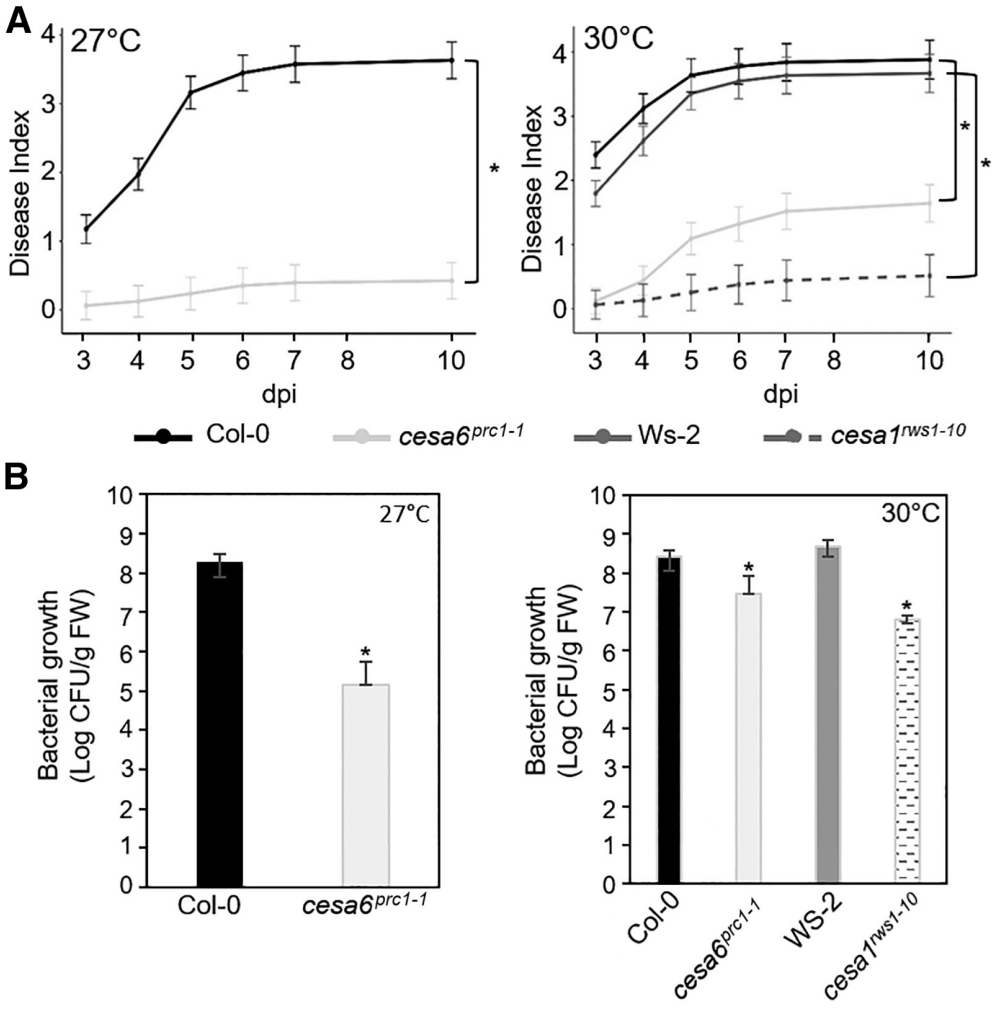

Fig. 7. *cesa1*$^{rws1\text{-}10}$ and *cesa6*$^{prc1\text{-}1}$ mutants affect disease symptoms and bacterial proliferation after inoculation with *Ralstonia solanacearum* GMI000 strain. **A,** Four-week-old plants were root-inoculated with *R. solanacearum* GMI1000, and disease symptoms were monitored after exposure to 27°C (for Col-0 and *cesa6*$^{prc1\text{-}1}$ mutant) or 30°C for the wild-type Ws-2 or Col-0 and the *cesa1*$^{rws1\text{-}10}$ or cesa6$^{prc1\text{-}1}$ respective mutant. Curves represent the least-square-means (lsmeans) ± standard errors of the lsmeans from three independent experiments. Pairwise differences were assessed based on area under the disease curve (AUC) values. Significant differences are indicated by asterisks (*) ($P < 0.001$). **B,** At 6 or 5 days postinoculation (dpi), the rosette of plants growing at 27 or 30°C, respectively, was recovered for bacterial counting. Bars represent the mean number ± standard errors of six plants per genotype and for three independent experiments. Significant differences to the corresponding wild-type genotype are represented by asterisks (*) ($P < 0.05$). FW, fresh weight.

previous studies showing that elevated temperatures support higher *R. solanacearum* population densities (Aoun et al. 2020; Wei et al. 2015). We cannot rule out the possibility that the greater bacterial colonization of roots at higher temperatures may contribute to the early onset of the plant response and/or disease.

The plant CW can function as a "passive/physical" defensive structure that many pathogens encounter before facing intracellular plant defenses (Lipka and Panstruga 2005; Underwood and Somerville 2008). Thus, the resistance of *cesa3^{mre1}* to *R. solanacearum* could be explained by the impact that the mutation has on the organization/architecture of the CW. Indeed, we found that depending on the *CESA3* allelic mutation, the CW can be differently affected, leading to different outcomes regarding pathogen infection (Lipka and Panstruga 2005; Underwood and Somerville 2008). Comparative analyses of root structure and composition, showing shorter swollen roots and expanded mature cortical cells in the cesa3^{mre1} mutant, support this hypothesis. Additionally, large-scale analysis of root tissues using FT-IR spectroscopy highlighted significant modifications of CW that might attest to significant alteration of root tissue organization or composition in the *cesa3^{mre1}* mutant compared with the Col-0 and *cesa3$^{ixr1\text{-}1}$* genotypes. Moreover, a rise in temperature did not modify the root cell organization and cortical cell width in *cesa3^{mre1}*, which remains resistant to *R. solanacearum* at 30°C, supporting the role that CW modification may play in plant resistance even at elevated temperatures. Data in the literature have shown that an increase in temperature (from 21 to 29°C) can result in a decrease in cellulose crystallinity and an increase in the velocity of CESA movement in the plasma membrane (Fujita et al. 2011). Whether the shift in temperature from 22 to 27 and 30°C in *cesa3^{mre1}* could have a differential impact on membrane fluidity that could contribute to a defense mechanism against the pathogen remains to be evaluated. We can speculate that the impact of the *cesa3^{mre1}* mutation on the CW and root cell architecture can modify the interaction with *R. solanacearum* and prevent the bacteria from breaking down this first barrier, thus impairing its spread across root tissues. Notably, in allowing the pathogen to have direct access to the xylem by cutting the roots before infection, we found a significant increase in susceptibility of *cesa3^{mre1}* plants to *R. solanacearum* at both 27 and 30°C, thus supporting this hypothesis. However, the appearance of wilting symptoms in *cesa3^{mre1}* was still delayed, which might imply that CW changes may have effects beyond their purely structural role.

Interestingly, the two other mutants tested (*cesa1$^{rsw1\text{-}10}$* and *cesa6$^{prc1\text{-}1}$*, which mutated in the two other subunits of the P-CW CSC, CESA1 and CESA6, respectively) both showed enhanced resistance to *R. solanacearum* at both 27 and 30°C. Similarly to *cesa3^{mre1}*, *cesa1$^{rsw1\text{-}10}$* has been shown to exhibit markedly reduced cellulose levels with defective root growth and a radially swelling phenotype. *cesa6$^{prc1\text{-}1}$* exhibits moderate deficiencies in root growth/phenotype and cellulose content (Desprez et al. 2002; Fagard et al. 2000). CESA1 and CESA3 are essential isoforms of the P-CW CESA complex, and their null mutants are

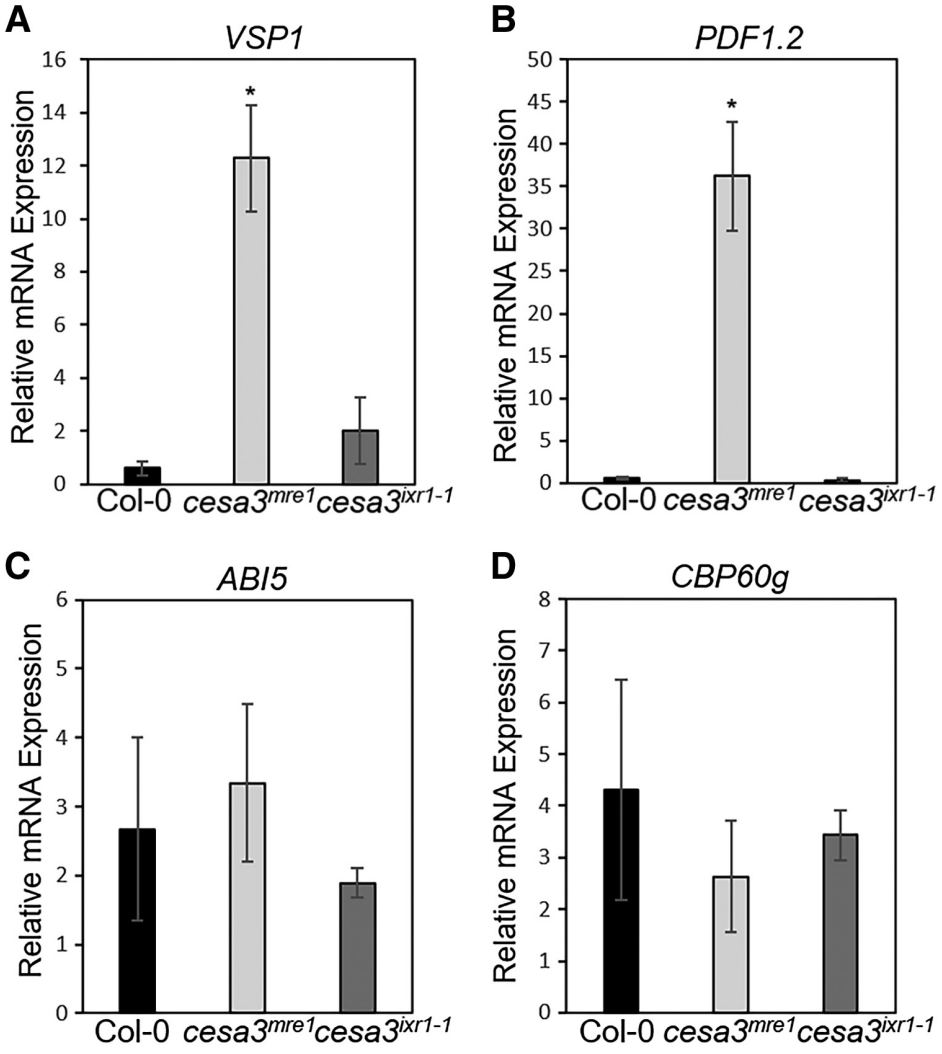

Fig. 8. Jasmonic acid-responsive genes are constitutively expressed in the *cesa3^{mre1}* mutant. Seven-day-old seedlings of the wild-type Col-0, *cesa3^{mre1}*, and *cesa3$^{ixr1\text{-}1}$* growing at 22°C were recovered for measurement of the relative mRNA level for **A,** *VSP1*, **B,** *PDF1.2*, **C,** *ABI5*, and **D,** *CBP60g* genes using reverse transcription-quantitative PCR and were normalized to the reference *EF-1α* At1G18070; $n = 3$ samples per genotype, with n consisting of 10 seedlings. Values are means ± standard errors, with asterisks (*) indicating statistically significant differences based on one-way analysis of variance ($P < 0.05$).

gamete lethal, whereas the CESA6 subunit may be redundant with other CESA6-related CESAs (Arioli et al. 1998; Desprez et al. 2007; Fagard et al. 2000; Persson et al. 2007). It has been evidenced that the three *CESA6*-like genes can only partially restore the altered phenotype in *cesa6*$^{prc1\text{-}1}$, thus showing partial redundancy of the *CESA6* gene (Desprez et al. 2007; Persson et al. 2007). Notably, the mutation site in *cesa6*$^{prc1\text{-}1}$ is localized in the class-specific region (CSR). This is an important region with potential for CESA isoform interactions that may be implicated in the specificity of the function of the CESA6 subunit and which might explain the resistant phenotype of the *cesa6*$^{prc1\text{-}1}$ mutant to *R. solanacearum* (Atanassov et al. 2009). In addition to the impact of the defects in *cesa1*$^{rsw1\text{-}10}$, *cesa3*^{mre1}, and *cesa6*$^{prc1\text{-}1}$ mutants on CW composition and root growth/development, we cannot exclude the possibility that these mutations affect CSC formation, stability or cellular trafficking of the P-CW CSC complex, or interaction with CESA-interacting proteins that modulate cellulose synthesis (Geisler et al. 2008; He et al. 2018; McFarlane et al. 2014; Speicher et al. 2018; Polko and Kieber 2019). Furthermore, how environmental cues such as bacterial infection or temperature changes could modulate CESAs' functions remains to be elucidated.

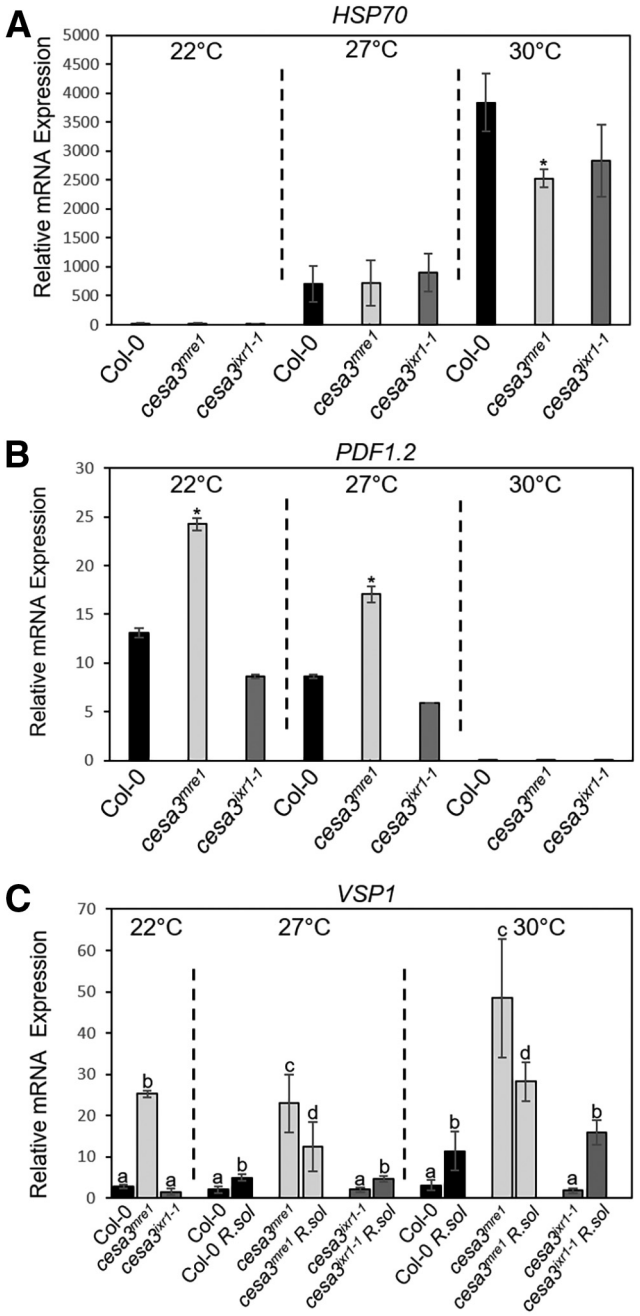

Fig. 9. *cesa3*^{mre1} enhances resistance to *Ralstonia solanacearum* at both 27 and 30°C and is associated with modulation of *VSP1* gene expression. Seven-day-old seedlings of wild-type Col-0, *cesa3*^{mre1}, and *cesa3*$^{ixr1\text{-}1}$ plants were transferred to the in vitro system on vertical Murashige and Skoog square plates. Roots were either left at 22°C or placed at 27 or 30°C. At 27 and 30°C, plants were mock inoculated or inoculated with *R. solanacearum* GMI1000 (*R.sol*). After 2 days, the relative mRNA expression level of **A,** *HSP70*; **B,** *PDF1.2*; and **C,** *VSP1* was measured by reverse transcription-quantitative PCR using the *EF-1*α At1G18070 as the reference gene. $n = 3$ biological samples per genotype per treatment, with each sample consisting of three independent roots. Values are means ± standard errors, with different letters indicating for each temperature condition statistically different results based on one-way analysis of variance ($P < 0.05$). Experiments were performed two times with similar results.

Several key mutants deficient in cellulose, such as *chitinase-like 1* (*ctl1*), *glycophosphatidylinositol* (*GPI*)*-linked COBRA* (*cob*), and *PM-bound endo-1,4-β-glucanase KORRIGAN1* (*kor1*), exhibit a dwarfed root phenotype (Nicol et al. 1998; Sánchez-Rodríguez et al. 2012; Schindelman et al. 2001). Intriguingly, along with the *cesa6*$^{prc1\text{-}1}$ and *cesa3* (*cesa3-3*) mutants, they all show increased resistance to the vascular fungal pathogen *F. oxysporum*, with resistance correlated to reduced root colonization by the fungus (Menna et al. 2021). However, in the case of the *ctl1-2* mutant, the dwarf root phenotype alone does not appear sufficient to explain the enhanced defense response (Menna et al. 2021). Another example linking a P-CW mutation leading to stunted roots and reduced cellulose content to biotic resistance was observed in the *cesa3*^{cev1} mutant against leaf biotrophic pathogens (Ellis and Turner 2001; Ellis et al. 2002a).

The role of the plant CW as a barrier inducing a defense response against biotic and abiotic stresses has long been recognized (Hamann et al. 2009; Ishida and Noutoshi 2022). Disruption of CWI can alter the condition of the CW and initiate defense mechanisms (Hématy et al. 2009; Hückelhoven 2007). Beyond its structural function, the plant CW thus serves as a relay for environmental information through signal transduction pathways (Hématy et al. 2009). Mutations in CESAs, whether affecting S-CW or S-CW formation, elicit various stress and defense responses, bolstering resistance against specific pathogens (Hématy et al. 2009). No clear evidence has been provided linking P-CW mutants, a dwarf root phenotype, and increased pathogen resistance at elevated temperatures. Nevertheless, the *radial swelling 1-1* mutant *cesa1*$^{rsw1\text{-}1}$, a temperature-sensitive mutant, shows reduced cellulose production at 31°C, causing severe defects in growth and morphogenesis (Arioli et al. 1998; Williamson et al. 2001).

The cellulose *cesa3*^{cev1} mutant shows constitutive ET and JA signaling and enhanced resistance to bacteria (*Pseudomonas syringae* pv. *maculicola*), fungi causing powdery mildew (*Erysiphe cichoracearum* UCSC1, *E. orontii* MGH, and *Oidium lycopersicum* Oxford), and aphids (*Myzus persicae*) (Ellis and Turner 2001; Ellis et al. 2002a). Additionally, defects in the S-CW CESAs (CESA4, CESA7, and CESA8) that lead to enhanced resistance to broad-host necrotrophic pathogens like the fungus *Plectosphaerella cucumerina* and *R. solanacearum* are associated with ABA-responsive, defense-related genes (Hernández-Blanco et al. 2007).

In this work, we found that the *cesa3*^{mre1} mutant constitutively expresses the JA-regulated gene *VSP1* and the ET- and JA-regulated gene *PDF1.2*. Interestingly, while a rise in temperature inhibits the expression of *PDF1.2*, it induces an upregulation in *VSP1* gene expression, which remains higher than that of both Col-0 and *cesa3*$^{ixr1\text{-}1}$ even in the presence of bacterial infection. The upregulation of JA signaling via *VSP1* could contribute

to a plant defense mechanism that hinders *R. solanacearum* during the early stages of bacterial infection beyond the major role as a physical barrier that the CW may play in *cesa3*^{mre1}.

Interestingly, the two other P-CW *cesa* mutants, *cesa1*$^{rsw1\text{-}10}$ and *cesa6*$^{prc1\text{-}1}$, showed constitutive expression of *VSP1* and *PDF1.2*, respectively (Caño-Delgado et al. 2003; Fagard et al. 2000), which is consistent with the hypothesis that resistance to *R. solanacearum* could be the result of the combined action of root structure and JA gene signaling.

Although JA is associated with plant defense against herbivory and necrotrophic pathogen attacks, emerging reports also associate JA with the positive regulation of plant immunity during biotrophic and hemibiotrophic pathogen infection, as suggested in the present study for *R. solanacearum* (Glazebrook 2005; Liu et al. 2016). For example, the JA-deficient tomato defenseless-1 (*def-1*) mutant plants displayed enhanced susceptibility to *P. syringae* pv *tomato* (DCT6D1) and *Xanthomonas campestris* pv. *vesicatoria* (DC93-1) (Thaler et al. 2004).

As far as we know, there is currently no evidence that VSP1 expression is regulated in response to *R. solanacearum*. However, within the context of the defense response linked to *R. solanacearum* effectors, it is noteworthy that *VSP1* exhibits a notable and differential upregulation, suggesting its involvement in PTI induction through its expression (Sohn et al. 2014).

In this scenario, we can hypothesize that in the *cesa3*^{mre1} mutant, alteration of CW integrity may trigger activation of signaling molecules (i.e., JA-responsive genes) that, combined with a structural defensive function, could contribute to reducing susceptibility to *R. solanacearum*.

Generally, temperature elevation has a drastic impact on *A. thaliana* defense responses to *R. solanacearum*, inhibiting the major source of resistance mediated by the immune-receptor pair RRS1-R/RPS4 (Aoun et al. 2017; Desaint et al. 2021). Thus, the role that *CESA3* plays in responding to *R. solanacearum* under heat stress conditions is particularly interesting, as it reveals resilient and robust resistance mechanisms against this pathogen in the current context of global warming.

In a broader context, these findings suggest that exploring natural allelic variants could be a promising avenue to uncover novel sources of adaptation to changing environments while preserving resistance to *R. solanacearum*.

Materials and Methods

Bacterial strain, plant material, and growth conditions

The GFP-expressing *R. solanacearum* GMI1000 strain (GMI1000 eGFP) was constructed by integrating the reporter gene in the chromosome downstream of glmS as previously described (Perrier et al. 2019). The wild-type GMI1000 and eGFP bacteria were grown in complete BG medium as described by Plener et al. (2010) that was supplemented, for the eGFP strain, with 10 μg of gentamicin. The five homozygous P-CW mutant plants used in this study, *cesa3*$^{ixr1\text{-}1}$, *cesa3*^{mre1}, *cesa1*$^{rsw1\text{-}10}$, *cesa6*^{prc1}, and *cesa3*$^{eli1\text{-}1}$, have been previously described (Arioli et al. 1998; Caño-Delgado et al. 2003; Desnos et al. 1996; Fagard et al. 2000; Pysh et al. 2012; Scheible et al. 2001). All mutants are in the Col-0 background, except for *cesa1*$^{rsw1\text{-}10}$, which originated from the Ws-2 background. Seeds were sterilized and plants were grown in a growth chamber under controlled conditions (22°C day/20°C night with 70% relative humidity [RH] and 16 h of light) as described previously (Deslandes et al. 2003).

Pathogenicity assay

For phenotyping and internal growth curve study, between 20 and 30 plantlets, depending on the experimental design, were transplanted in Jiffy pots (Jiffy Products International AS, Norway) and put in a growth chamber (22°C with 70% RH and 9 h of light) for 3 weeks. Plant infection with the GMI1000 strain was done as previously reported by inoculating roots with the bacterial suspension (10^8 colony-forming units [CFU]/ml) (Aoun et al. 2017; Deslandes et al. 2003). For direct infection of the xylem, roots were sectioned with scissors approximately 1 cm from the bottom of the Jiffy pot (Deslandes et al. 1998). Inoculated plants were transferred in growth chambers at 27 or 30°C (75% RH with 12 h of light; 100 μmol m^{-2} s^{-1}). At least 12 plants per genotype were inoculated in each of the two to three independent experiments for each temperature condition, and the disease rating means and SD were estimated at different times.

The wilting symptoms were scored on an established zero to four DI scale (Deslandes et al. 1998), with the scores 0 and 4 corresponding to healthy and dead plants, respectively (Supplementary Fig. S2). Symptoms were monitored from 3 to 10 dpi. For in planta bacterial growth curves, samples were recovered at the time with a Col-0 DI mean of around 1 and performed as described (Deslandes et al. 1998).

In vitro plant growth assay

For microscopy, bacterial count, and qPCR analysis in roots, plantlets were transferred to 12- × 12-cm Petri dishes containing modified MS medium ($MgSO_4$ concentration increased to 3 mM) and 0.5% Phytagel (Sigma), supplemented with 50 nM of 2-amino ethoxyvinyl Gly (AVG). The AVG is included to limit ethylene production (Guinel and Geil 2002). Roots were covered with a sterile, gas-permeable, and transparent plastic film (BioFolie 25; Sartorius AG, Vivascience), which has the same optical refractive index as water. This allows the use of water-immersion objectives for in vivo observation, limits water evaporation from the plates during observation, and reduces the risk of contamination of the roots (Fournier et al. 2008). Plants were grown vertically in the culture room with the plates slightly tilted to favor the growth of roots along the plastic film and with the roots protected from light using black paper bags. Inoculation with GMI1000 expressing eGFP was performed by spotting an aqueous suspension of exponentially growing bacteria (approximately 10^7 CFU/ml) 1 cm above the root apex between the plastic foil and the semisolid medium (Digonnet et al. 2012).

Calcofluor staining

For Calcofluor staining, plantlets of *A. thaliana* were grown in vitro as described above, and roots were recovered 10 days after exposure to 22, 27, and 30°C. Roots were fixed for 2 days in ethanol 70%). For each genotype and condition, four to seven independent roots were used in each of three independent experiments. Root sections approximately 1 cm in length, taken from the apex region, were grouped according to repetition and genotype. These sections were embedded in 2% low melting point (LMP) agarose before undergoing dehydration with increasing concentrations of ethanol up to 100%. Following dehydration, the sections were embedded in an acrylic resin using a graded series of ethanol/LRWhite resin mixtures (EtOH/LRW 3:1, 2:2, 1:3, and finally 100% LRWhite resin). Thin sections (1 μm) were placed on PTFE printed slides (Electron Microscopy Sciences) and labeled in Calcofluor White for cellulose staining.

Sections were incubated at room temperature for 3 min with a solution of 0.1% Calcofluor. Slides were then washed with deionized water and dried under a stream of dry air.

Confocal microscopy

For visualization of Calcofluor-stained roots, images of root sections (1-μm thickness) were acquired with a spectral confocal laser scanning system (SP8, Leica, Germany) equipped with an upright microscope (DM6000, Leica, Germany). Observations were made using a 40× (HC PL APO N.A. 1.3) oil immersion

objective. A laser diode emitted at 405 nm was used to collect the fluorescence of the cellulose (β1-4 glucans) in the range between 415 to 485 nm.

Biochemical analyses of S-CWs

For FT-IR absorption spectra, plants were grown in vitro in square plates as previously described for 15 days. Roots from 14 plants/genotype and the condition of two independent experiments were recovered, and soluble extracts were eliminated as described by Ployet et al. (2019). Briefly, samples were freeze-dried for 48 h, ground using a Mixer Mill MM 400 (Retsch GmbH, Haan, Germany), and extracted by hot solvents (successively water, ethanol, and ethanol/toluene [1:1 v/v] and acetone) to obtain extractive-free root samples (EFR). FT-IR analysis was performed on 100 to 200 mg of EFR. Spectra were recorded from 10 technical replicates in the range of 400 to 4,000 cm^{-1} with a 4-cm^{-1} resolution and 32 scans/spectrum using an attenuated total reflection (ATR) Nicolet 6700 FT-IR spectrometer (Thermo Fisher, Illkirch-Graffenstaden, France) equipped with a deuterated-triglycine sulphate (DTGS) detector. Spectra analyses were performed as described in Dai et al. (2020).

Cellulose quantification

Roots from 14 plants/genotype and the condition of plants grown in vitro in square plates for 15 days were recovered and placed in two volumes of 96% ethanol. Two independent experiments were performed. Once the ethanol had been removed, the roots were dried and ground; 10 mg of alcohol insoluble residues (AIR) were weighed and digested in 50-mM sodium acetate buffer in the presence of 500 U/ml of a-amylase (Megazyme Inc) for 5 h. Two volumes of ethanol were added, and after centrifugation, the supernatant was discarded; 400 ml of freshly made 2M trifluoroacetic acid (TFA) was added to the pellet. The samples were placed for 1 h at 120°C and centrifuged at 4°C for 15 min at 14,000 rpm. The supernatant was discarded, and the pellet was washed twice with 70% ethanol before drying. To obtain the glucose content of the crystalline cellulose fraction, the TFA-insoluble pellet was hydrolyzed with 72% (v/v) sulfuric acid for 1 h at room temperature. The sulfuric acid was then diluted to 1 M with water, and the samples were incubated at 100°C for 3 h. All samples were filtered using 20-μm filter caps and quantified by high performance anion-exchange chromatography coupled with pulsed amperometric detection (HPAEC-PAD) on a Dionex ICS-5000 instrument (Thermo Fisher Scientific). The experiment was repeated three times for each genotype and temperature, showing comparable differences in values among the three genotypes.

Expression analysis

Col-0, *cesa3*^{mre1}, and *cesa3*$^{ixr1\text{-}1}$ were grown on square plates for 7 days and were left at 22°C or exposed to 27 or 30°C as control or upon infection with the GMI1000 eGFP strain. Four roots per genotype for each condition of three independent experiments were recovered and flash-frozen for RNA extraction. Material was ground to a fine powder using a Mixer Mill MM 400 (Retsch), and RNA extraction was performed following the NucleoSpin RNA plus protocol provided with the DNA, RNA, and Protein Purification kit (Macherey-Nagel, Düren, Germany). Moloney Murine Leukemia Virus Reverse Transcriptase (M-MLV RT) (Life Technologies) was used to synthetize cDNA. For all genes of interest, 100 ng of cDNA template was used for quantitative PCR (qPCR) with gene-specific primers (Supplementary Table S3) and presented as relative expression to the *EF-1*α internal control gene.

Local score analysis

A local score approach was implemented on the set of *P* values provided by Efficient Mixed-Model Association eXpedited (EMMAX) in Aoun et al. (2017) GWA data following Bonhomme et al. (2019). After several preliminary tests, the parameter controlling QTL detection stringency was set at $\xi = 2$. The local score analysis defines intervals of physical positions in the genome, in which the association between this genomic region and the trait is statistically significant. These significant zones will be hereafter called QTLs. The QTLs from all "time point × temperature treatment" combination where the "accession" effect was significant (Aoun et al. 2017) were taken into consideration. If physical positions of QTLs identified in different combinations overlapped, a new QTL was defined encompassing both original QTLs. QTLs limits were compared with the gene's limits annotated in the 10th version of the genome provided by the Arabidopsis International Resource (TAIR 10; http://www.arabidopsis.org). Two situations arose: (i) if a QTL's limits overlap with a gene's limits, the gene is considered as a candidate under 'strict condition'; (ii) if a QTL's limits fall in a 2-kbp distance before or after the gene, the gene is considered as a candidate under the 'lenient condition'. This second condition considers the possibility of the QTL to be put into a gene-promoter region or considers the presence of longer and overlooked LD. In terms of priority, the 'strict condition' takes precedence over the 'lenient condition'.

Disease ratings analysis

For each time point (dpi) at each condition (a specific combination of temperature [27 or 30°C] and root status [cut or uncut]), disease ratings were adjusted using the following linear model:

$$Y_{i,j,k} = \mu + \alpha_i + \beta_j + \gamma_{i,j} + \varepsilon_{i,j,k}$$

where $Y_{i,j,k}$ denotes the phenotype of the k^{th} plant of the j^{th} replicate of the i^{th} genotype; μ is the intercept; α is the genotypic fixed effect; β is the replicate fixed effect; γ is the replicate × genotype interaction fixed effects; and ε are the residuals with $\varepsilon_{i,j,k} \hookrightarrow N(0, \sigma^2_\varepsilon)$ independently and identically distributed. Least-square-means (lsmeans) of the genotypic effect and their associated confidence intervals (confidence level of 0.95) were obtained using the linear model. Contrast tests were made between each pair of genotypes. The R package *emmeans* was used to compute lsmeans and to perform contrast tests.

Area under the disease curve (AUC)

AUC of each plant curve was computed using both right- and left-rectangle methods. The final AUC value was the mean between values obtained using these two methods. These AUC values were used, separately for each condition, as the new phenotype to adjust the linear model and to compute lsmeans.

Day of appearance of the first symptoms

To assess if a genotype tends to present disease symptoms earlier than others, the day of appearance of the first symptoms (d_0) was computed. This was built as $d_0 = min_t(Y_{i,j,k}(t) > 0)$, indicating when the first day (for each plant) when the phenotypic disease rating is strictly above 0. Because the experiment ended at 10 dpi, plants presenting no disease symptoms during the 10 dpi were arbitrary set at $d_0 = 11$. A similar procedure as described in the previous paragraph using d_0 as the new phenotype was used to adjust the linear model and to compute lsmeans.

Acknowledgments

We are grateful to L. Deslandes, M. Bernoux, and D. Tremousaygue for helpful discussions. This work has benefited from the support of the Institut Jean-Pierre Bourgin (IJPB)'s plant observatory technological platforms, especially the chemistry platform (Gregory Mouille and Salem Chabout).

Literature Cited

Adamafio, N. A., Kyeremeh, K., Datsomor, A., and Osei-Owusu, J. 2013. Cocoa pod ash pre-treatment of wawa (*Triplochiton scleroxylon*) and sapele (*Entandrophragma cylindricum*) sawdust: Fourier transform infrared spectroscopic characterization of lignin. Asian J. Sci. Res. 6:812-818.

Alonso-Simón, A., García-Angulo, P., Mélida, H., Encina, A., Álvarez, J. M., and Acebes, J. L. 2011. The use of FTIR spectroscopy to monitor modifications in plant cell wall architecture caused by cellulose biosynthesis inhibitors. Plant Signal. Behav. 6:1104-1110.

Aoun, N., Desaint, H., Boyrie, L., Bonhomme, M., Deslandes, L., Berthomé, R., and Roux, F. 2020. A complex network of additive and epistatic quantitative trait loci underlies natural variation of *Arabidopsis thaliana* quantitative disease resistance to *Ralstonia solanacearum* under heat stress. Mol. Plant Pathol. 21:1405-1420.

Aoun, N., Tauleigne, L., Lonjon, F., Deslandes, L., Vailleau, F., Roux, F., and Berthomé, R. 2017. Quantitative disease resistance under elevated temperature: Genetic basis of new resistance mechanisms to *Ralstonia solanacearum*. Front. Plant Sci. 8:1387.

Arioli, T., Peng, L., Betzner, A. S., Burn, J., Wittke, W., Herth, W., Camilleri, C., Höfte, H., Plazinski, J., Birch, R., Cork, A., Glover, J., Redmond, J., and Williamson, R. E. 1998. Molecular analysis of cellulose biosynthesis in *Arabidopsis*. Science 279:717-720.

Atanassov, I. I., Pittman, J. K., and Turner, S. R. 2009. Elucidating the mechanisms of assembly and subunit interaction of the cellulose synthase complex of *Arabidopsis* secondary cell walls. J. Biol. Chem. 284:3833-3841.

Bacete, L., Mélida, H., López, G., Dabos, P., Tremousaygue, D., Denancé, N., Miedes, E., Bulone, V., Goffner, D., and Molina, A. 2020. *Arabidopsis* response regulator 6 (ARR6) modulates plant cell-wall composition and disease resistance. Mol. Plant-Microbe Interact. 33:767-780.

Bacete, L., Mélida, H., Miedes, E., and Molina, A. 2018. Plant cell wall-mediated immunity: Cell wall changes trigger disease resistance responses. Plant J. 93:614-636.

Bebber, D. P., Ramotowski, M. A. T., and Gurr, S. J. 2013. Crop pests and pathogens move polewards in a warming world. Nat. Clim. Change 3:985-988.

Bonhomme, M., Fariello, M. I., Navier, H., Hajri, A., Badis, Y., Miteul, H., Samac, D. A., Dumas, B., Baranger, A., Jacquet, C., and Pilet-Nayel, M.-L. 2019. A local score approach improves GWAS resolution and detects minor QTL: Application to *Medicago truncatula* quantitative disease resistance to multiple *Aphanomyces euteiches* isolates. Heredity 123:517-531.

Caño-Delgado, A., Penfield, S., Smith, C., Catley, M., and Bevan, M. 2003. Reduced cellulose synthesis invokes lignification and defense responses in *Arabidopsis thaliana*. Plant J. 34:351-362.

Casas, A., Alonso, M. V., Oliet, M., Rojo, E., and Rodríguez, F. 2012. FTIR analysis of lignin regenerated from *Pinus radiata* and *Eucalyptus globulus* woods dissolved in imidazolium-based ionic liquids. J. Chem. Technol. Biotechnol. 87:472-480.

Chen, Z., Hong, X., Zhang, H., Wang, Y., Li, X., Zhu, J.-K., and Gong, Z. 2005. Disruption of the cellulose synthase gene, *AtCesA8/IRX1*, enhances drought and osmotic stress tolerance in *Arabidopsis*. Plant J. 43:273-283.

Couto, D., and Zipfel, C. 2016. Regulation of pattern recognition receptor signalling in plants. Nat. Rev. Immunol. 16:537-552.

Czechowski, T., Stitt, M., Altmann, T., Udvardi, M. K., and Scheible, W.-R. 2005. Genome-wide identification and testing of superior reference genes for transcript normalization in *Arabidopsis*. Plant Physiol. 139:5-17.

Dai, Y., Hu, G., Dupas, A., Medina, L., Blandels, N., San Clemente, H., Ladouce, N., Badawi, M., Hernandez-Raquet, G., Mounet, F., Grima-Pettenati, J., and Cassan-Wang, H. 2020. Implementing the CRISPR/Cas9 technology in *Eucalyptus* hairy roots using wood-related genes. Int. J. Mol. Sci. 21:3408.

Desaint, H., Aoun, N., Deslandes, L., Vailleau, F., Roux, F., and Berthomé, R. 2021. Fight hard or die trying: When plants face pathogens under heat stress. New Phytol. 229:712-734.

Deslandes, L., Olivier, J., Peeters, N., Feng, D. X., Khounlotham, M., Boucher, C., Somssich, I., Genin, S., and Marco, Y. 2003. Physical interaction between RRS1-R, a protein conferring resistance to bacterial wilt, and PopP2, a type III effector targeted to the plant nucleus. Proc. Natl. Acad. Sci. U.S.A. 100:8024-8029.

Deslandes, L., Olivier, J., Theulières, F., Hirsch, J., Feng, D. X., Bittner-Eddy, P., Beynon, J., and Marco, Y. 2002. Resistance to *Ralstonia solanacearum* in *Arabidopsis thaliana* is conferred by the recessive *RRS1-R* gene, a member of a novel family of resistance genes. Proc. Natl. Acad. Sci. U.S.A. 99:2404-2409.

Deslandes, L., Pileur, F., Liaubet, L., Camut, S., Can, C., Williams, K., Holub, E., Beynon, J., Arlat, M., and Marco, Y. 1998. Genetic characterization of *RRS1*, a recessive locus in *Arabidopsis thaliana* that confers resistance to the bacterial soilborne pathogen *Ralstonia solanacearum*. Mol. Plant-Microbe Interact. 11:659-667.

Desnos, T., Orbović, V., Bellini, C., Kronenberger, J., Caboche, M., Traas, J., and Höfte, H. 1996. *Procuste1* mutants identify two distinct genetic pathways controlling hypocotyl cell elongation, respectively in dark- and light-grown *Arabidopsis* seedlings. Development 122:683-693.

Desprez, T., Juraniec, M., Crowell, E. F., Jouy, H., Pochylova, Z., Parcy, F., Höfte, H., Gonneau, M., and Vernhettes, S. 2007. Organization of cellulose synthase complexes involved in primary cell wall synthesis in *Arabidopsis thaliana*. Proc. Natl. Acad. Sci. U.S.A. 104:15572-15577.

Desprez, T., Vernhettes, S., Fagard, M., Refrégier, G., Desnos, T., Aletti, E., Py, N., Pelletier, S., and Höfte, H. 2002. Resistance against herbicide isoxaben and cellulose deficiency caused by distinct mutations in the same cellulose synthase isoform CESA6. Plant Physiol. 128:482-490.

Digonnet, C., Martinez, Y., Denancé, N., Chasseray, M., Dabos, P., Ranocha, P., Marco, Y., Jauneau, A., and Goffner, D. 2012. Deciphering the route of *Ralstonia solanacearum* colonization in *Arabidopsis thaliana* roots during a compatible interaction: Focus on the plant cell wall. Planta 236:1419-1431.

Ding, L.-N., Li, Y.-T., Wu, Y.-Z., Li, T., Geng, R., Cao, J., Zhang, W., and Tan, X.-L. 2022. Plant disease resistance-related signaling pathways: Recent progress and future prospects. Int. J. Mol. Sci. 23:16200.

Ellis, C., Karafyllidis, I., and Turner, J. G. 2002a. Constitutive activation of jasmonate signaling in an *Arabidopsis* mutant correlates with enhanced resistance to *Erysiphe cichoracearum*, *Pseudomonas syringae*, and *Myzus persicae*. Mol. Plant-Microbe Interact. 15:1025-1030.

Ellis, C., Karafyllidis, I., Wasternack, C., and Turner, J. G. 2002b. The Arabidopsis mutant *cev1* links cell wall signaling to jasmonate and ethylene responses. Plant Cell 14:1557-1566.

Ellis, C., and Turner, J. G. 2001. The *Arabidopsis* mutant *cev1* has constitutively active jasmonate and ethylene signal pathways and enhanced resistance to pathogens. Plant Cell 13:1025-1033.

Fagard, M., Desnos, T., Desprez, T., Goubet, F., Refregier, G., Mouille, G., McCann, M., Rayon, C., Vernhettes, S., and Höfte, H. 2000. *PROCUSTE1* encodes a cellulose synthase required for normal cell elongation specifically in roots and dark-grown hypocotyls of Arabidopsis. Plant Cell 12:2409-2423.

Fleischer, T., Gampe, J., Scheuerlein, A., and Kerth, G. 2017. Rare catastrophic events drive population dynamics in a bat species with negligible senescence. Sci. Rep. 7:7370.

Fournier, J., Timmers, A. C. J., Sieberer, B. J., Jauneau, A., Chabaud, M., and Barker, D. G. 2008. Mechanism of infection thread elongation in root hairs of *Medicago truncatula* and dynamic interplay with associated rhizobial colonization. Plant Physiol. 148:1985-1995.

Fujita, M., Himmelspach, R., Hocart, C. H., Williamson, R. E., Mansfield, S. D., and Wasteneys, G. O. 2011. Cortical microtubules optimize cell-wall crystallinity to drive unidirectional growth in Arabidopsis. Plant J. 66:915-928.

Geisler, D. A., Sampathkumar, A., Mutwil, M., and Persson, S. 2008. Laying down the bricks: Logistic aspects of cell wall biosynthesis. Curr. Opin. Plant Biol. 11:647-652.

Glazebrook, J. 2005. Contrasting mechanisms of defense against biotrophic and necrotrophic pathogens. Ann. Rev. Phytopathol. 43:205-227.

Gonneau, M., Desprez, T., Martin, M., Doblas, V. G., Bacete, L., Miart, F., Sormani, R., Hématy, K., Renou, J., Landrein, B., Murphy, E., Van De Cotte, B., Vernhettes, S., De Smet, I., and Höfte, H. 2018. Receptor kinase THESEUS1 is a rapid alkalinization factor 34 receptor in *Arabidopsis*. Curr. Biol. 28:2452-2458.e4.

Guinel, F. C., and Geil, R. D. 2002. A model for the development of the rhizobial and arbuscular mycorrhizal symbioses in legumes and its use to understand the roles of ethylene in the establishment of these two symbioses. Can. J. Bot. 80:695-720.

Hamann, T. 2012. Plant cell wall integrity maintenance as an essential component of biotic stress response mechanisms. Front. Plant Sci. 3:77.

Hamann, T., Bennett, M., Mansfield, J., and Somerville, C. 2009. Identification of cell-wall stress as a hexose-dependent and osmosensitive regulator of plant responses. Plant J. 57:1015-1026.

Harris, D. M., Corbin, K., Wang, T., Gutierrez, R., Bertolo, A. L., Petti, C., Smilgies, D.-M., Estevez, J. M., Bonetta, D., Urbanowicz, B. R., Ehrhardt, D. W., Somerville, C. R., Rose, J. K. C., Hong, M., and DeBolt, S. 2012. Cellulose microfibril crystallinity is reduced by mutating C-terminal transmembrane region residues $CESA1^{A903V}$ and $CESA3^{T942I}$ of cellulose synthase. Proc. Natl. Acad. Sci. U.S.A. 109:4098-4103.

He, M., Lan, M., Zhang, B., Zhou, Y., Wang, Y., Zhu, L., Yuan, M., and Fu, Y. 2018. Rab-H1b is essential for trafficking of cellulose synthase and for hypocotyl growth in *Arabidopsis thaliana*. J. Integr. Plant Biol. 60:1051-1069.

Heim, D. R., Roberts, J. L., Pike, P. D., and Larrinua, I. M. 1989. Mutation of a locus of *Arabidopsis thaliana* confers resistance to the herbicide isoxaben. Plant Physiol. 90:146-150.

Hématy, K., Cherk, C., and Somerville, S. 2009. Host-pathogen warfare at the plant cell wall. Curr. Opin. Plant Biol. 12:406-413.

Hernández-Blanco, C., Feng, D. X., Hu, J., Sánchez-Vallet, A., Deslandes, L., Llorente, F., Berrocal-Lobo, M., Keller, H., Barlet, X., Sánchez-Rodríguez, C., Anderson, L. K., Somerville, S., Marco, Y., and Molina, A. 2007. Impairment of cellulose synthases required for *Arabidopsis* secondary cell wall formation enhances disease resistance. Plant Cell 19:890-903.

Hill, J. L., Jr., Hammudi, M. B., and Tien, M. 2014. The *Arabidopsis* cellulose synthase complex: A proposed hexamer of CESA trimers in an equimolar stoichiometry. Plant Cell 26:4834-4842.

Höfte, H., and Voxeur, A. 2017. Plant cell walls. Curr. Biol. 27:R865-R870.

Hu, Z., Vanderhaeghen, R., Cools, T., Wang, Y., De Clercq, I., Leroux, O., Nguyen, L., Belt, K., Millar, A. H., Audenaert, D., Hilson, P., Small, I., Mouille, G., Vernhettes, S., Van Breusegem, F., Whelan, J., Höfte, H., and De Veylder, L. 2016. Mitochondrial defects confer tolerance against cellulose deficiency. Plant Cell 28:2276-2290.

Hückelhoven, R. 2007. Cell wall-associated mechanisms of disease resistance and susceptibility. Ann. Rev. Phytopathol. 45:101-127.

Huot, B., Castroverde, C. D. M., Velásquez, A. C., Hubbard, E., Pulman, J. A., Yao, J., Childs, K. L., Tsuda, K., Montgomery, B. L., and He, S. Y. 2017. Dual impact of elevated temperature on plant defence and bacterial virulence in *Arabidopsis*. Nat. Comm. 8:1808.

IPCC. 2022. Climate Change 2022: Mitigation of Climate Change. Contribution of Working Group III to the Sixth Assessment Report of the Intergovernmental Panel on Climate Change. P. R. Shukla, J. Skea, R. Slade, A. Al Khourdajie, R. van Diemen, D. McCollum, M. Pathak, S. Some, P. Vyas, R. Fradera, M. Belkacemi, A. Hasija, G. Lisboa, S. Luz, and J. Malley, eds. Cambridge University Press, Cambridge, U.K.

Ishida, K., and Noutoshi, Y. 2022. The function of the plant cell wall in plant-microbe interactions. Plant Physiol. Biochem. 192:273-284.

Ji, D., Chen, T., Zhang, Z., Li, B., and Tian, S. 2020. Versatile roles of the receptor-like kinase Feronia in plant growth, development and host-pathogen interaction. Int. J. Mol. Sci. 21:7881.

Kessler, S. A., Shimosato-Asano, H., Keinath, N. F., Wuest, S. E., Ingram, G., Panstruga, R., and Grossniklaus, U. 2010. Conserved molecular components for pollen tube reception and fungal invasion. Science 330:968-971.

Largo-Gosens, A., Hernández-Altamirano, M., García-Calvo, L., Alonso-Simón, A., Álvarez, J., and Acebes, J. L. 2014. Fourier transform mid infrared spectroscopy applications for monitoring the structural plasticity of plant cell walls. Front. Plant Sci. 5:303.

Lipka, V., and Panstruga, R. 2005. Dynamic cellular responses in plant-microbe interactions. Curr. Opin. Plant Biol. 8:625-631.

Liu, L., Sonbol, F.-M., Huot, B., Gu, Y., Withers, J., Mwimba, M., Yao, J., He, S. Y., and Dong, X. 2016. Salicylic acid receptors activate jasmonic acid signalling through a non-canonical pathway to promote effector-triggered immunity. Nat. Comm. 7:13099.

Lobell, D. B., Schlenker, W., and Costa-Roberts, J. 2011. Climate trends and global crop production since 1980. Science 333:616-620.

Lorrai, R., and Ferrari, S. 2021. Host cell wall damage during pathogen infection: Mechanisms of perception and role in plant-pathogen interactions. Plants 10:399.

McFarlane, H. E., Döring, A., and Persson, S. 2014. The cell biology of cellulose synthesis. Ann. Rev. Plant Biol. 65:69-94.

Menna, A., Dora, S., Sancho-Andrés, G., Kashyap, A., Meena, M. K., Sklodowski, K., Gasperini, D., Coll, N. S., and Sánchez-Rodríguez, C. 2021. A primary cell wall cellulose-dependent defense mechanism against vascular pathogens revealed by time-resolved dual transcriptomics. BMC Biol. 19:161.

Moat, J., Gole, T. W., and Davis, A. P. 2019. Least concern to endangered: Applying climate change projections profoundly influences the extinction risk assessment for wild Arabica coffee. Glob. Change Biol. 25: 390-403.

Mouille, G., Robin, S., Lecomte, M., Pagant, S., and Höfte, H. 2003. Classification and identification of *Arabidopsis* cell wall mutants using Fourier-Transform InfraRed (FT-IR) microspectroscopy. Plant J. 35:393-404.

Nicol, F., His, I., Jauneau, A., Vernhettes, S., Canut, H., and Höfte, H. 1998. A plasma membrane-bound putative endo-1,4-β-D-glucanase is required for normal wall assembly and cell elongation in *Arabidopsis*. EMBO J. 17:5563-5576.

Panstruga, R., and Dodds, P. N. 2009. Terrific protein traffic: The mystery of effector protein delivery by filamentous plant pathogens. Science 324:748-750.

Pastor, V., Cervero, R., and Gamir, J. 2022. The simultaneous perception of self- and non-self-danger signals potentiates plant innate immunity responses. Planta 256:10.

Perrier, A., Barlet, X., Rengel, D., Prior, P., Poussier, S., Genin, S., and Guidot, A. 2019. Spontaneous mutations in a regulatory gene induce phenotypic heterogeneity and adaptation of *Ralstonia solanacearum* to changing environments. Environ. Microbiol. 21:3140-3152.

Persson, S., Paredez, A., Carroll, A., Palsdottir, H., Doblin, M., Poindexter, P., Khitrov, N., Auer, M., and Somerville, C. R. 2007. Genetic evidence for three unique components in primary cell-wall cellulose synthase complexes in *Arabidopsis*. Proc. Natl. Acad. Sci. U.S.A. 104:15566-15571.

Planas-Marquès, M., Kressin, J. P., Kashyap, A., Panthee, D. R., Louws, F. J., Coll, N. S., and Valls, M. 2020. Four bottlenecks restrict colonization and invasion by the pathogen *Ralstonia solanacearum* in resistant tomato. J. Exp. Bot. 71:2157-2171.

Plener, L., Manfredi, P., Valls, M., and Genin, S. 2010. PrhG, a transcriptional regulator responding to growth conditions, is involved in the control of the type III secretion system regulon in *Ralstonia solanacearum*. J. Bacteriol. 192:1011-1019.

Ployet, R., Veneziano Labate, M. T., Regiani Cataldi, T., Christina, M., Morel, M., San Clemente, H., Denis, M., Favreau, B., Tomazello Filho, M., Laclau, J.-P., Labate, C. A., Chaix, G., Grima-Pettenati, J., and Mounet, F. 2019. A systems biology view of wood formation in *Eucalyptus grandis* trees submitted to different potassium and water regimes. New Phytol. 223:766-782.

Polko, J. K., and Kieber, J. J. 2019. The regulation of cellulose biosynthesis in plants. Plant Cell 31:282-296.

Pysh, L., Alexander, N., Swatzyna, L., and Harbert, R. 2012. Four alleles of *AtCESA3* form an allelic series with respect to root phenotype in *Arabidopsis thaliana*. Physiol. Plant. 144:369-381.

Ramírez, V., Agorio, A., Coego, A., García-Andrade, J., Hernández, M. J., Balaguer, B., Ouwerkerk, P. B. F., Zarra, I., and Vera, P. 2011. MYB46 modulates disease susceptibility to *Botrytis cinerea* in Arabidopsis. Plant Physiol. 155:1920-1935.

Renou, J., Li, D., Lu, J., Zhang, B., Gineau, E., Ye, Y., Shi, J., Voxeur, A., Akary, E., Marmagne, A., Gonneau, M., Uyttewaal, M., Höfte, H., Zhao, Y., and Vernhettes, S. 2024. A cellulose synthesis inhibitor affects cellulose synthase complex secretion and cortical microtubule dynamics. Plant Physiol. 4:kiae232.

Rosenzweig, C., Elliott, J., Deryng, D., Ruane, A. C., Müller, C., Arneth, A., Boote, K. J., Folberth, C., Glotter, M., Khabarov, N., Neumann, K., Piontek, F., Pugh, T. A. M., Schmid, E., Stehfest, E., Yang, H., and Jones, J. W. 2014. Assessing agricultural risks of climate change in the 21st century in a global gridded crop model intercomparison. Proc. Natl. Acad. Sci. U.S.A. 111:3268-3273.

Rui, Y., and Dinneny, J. R. 2020. A wall with integrity: Surveillance and maintenance of the plant cell wall under stress. New Phytol. 225:1428-1439.

Saijo, Y., and Loo, E. P.-i. 2020. Plant immunity in signal integration between biotic and abiotic stress responses. New Phytol. 225:87-104.

Sammons, R. J., Harper, D. P., Labbé, N., Bozell, J. J., Elder, T., and Rials, T. G. 2013. Characterization of organosolv lignins using thermal and FT-IR spectroscopic analysis. BioResources 8:2752-2767.

Sánchez-Rodríguez, C., Bauer, S., Hématy, K., Saxe, F., Ibáñez, A. B., Vodermaier, V., Konlechner, C., Sampathkumar, A., Rüggeberg, M., Aichinger, E., Neumetzler, L., Burgert, I., Somerville, C., Hauser, M.-T., and Persson, S. 2012. CHITINASE-LIKE1/POM-POM1 and its homolog CTL2 are glucan-interacting proteins important for cellulose biosynthesis in *Arabidopsis*. Plant Cell 24:589-607.

Sánchez-Vallet, A., López, G., Ramos, B., Delgado-Cerezo, M., Riviere, M.-P., Llorente, F., Fernández, P. V., Miedes, E., Estevez, J. M., Grant, M., and Molina, A. 2012. Disruption of abscisic acid signaling constitutively activates Arabidopsis resistance to the necrotrophic fungus *Plectosphaerella cucumerina*. Plant Physiol. 160:2109-2124.

Scheible, W.-R., Eshed, R., Richmond, T., Delmer, D., and Somerville, C. 2001. Modifications of cellulose synthase confer resistance to isoxaben and thiazolidinone herbicides in *Arabidopsis Ixr1* mutants. Proc. Natl. Acad. Sci. U.S.A. 98:10079-10084.

Schindelman, G., Morikami, A., Jung, J., Baskin, T. I., Carpita, N. C., Derbyshire, P., McCann, M. C., and Benfey, P. N. 2001. COBRA encodes a putative GPI-anchored protein, which is polarly localized and necessary for oriented cell expansion in *Arabidopsis*. Genes Dev. 15: 1115-1127.

Sethaphong, L., Haigler, C. H., Kubicki, J. D., Zimmer, J., Bonetta, D., DeBolt, S., and Yingling, Y. G. 2013. Tertiary model of a plant cellulose synthase. Proc. Natl. Acad. Sci. U.S.A. 110:7512-7517.

Shim, I., Law, R., Kileeg, Z., Stronghill, P., Northey, J. G. B., Strap, J. L., and Bonetta, D. T. 2018. Alleles causing resistance to isoxaben and flupoxam

highlight the significance of transmembrane domains for CESA protein function. Front. Plant Sci. 9:1152.
Sohn, K. H., Segonzac, C., Rallapalli, G., Sarris, P. F., Woo, J. Y., Williams, S. J., Newman, T. E., Paek, K. H., Kobe, B., and Jones, J. D. G. 2014. The nuclear immune receptor *RPS4* is required for *RRS1*^{SLH1}-dependent constitutive defense activation in *Arabidopsis thaliana*. PLoS Genet. 10:e1004655.
Speicher, T. L., Li, P. Z., and Wallace, I. S. 2018. Phosphoregulation of the plant cellulose synthase complex and cellulose synthase-like proteins. Plants 7:52.
Stark, N. M., Yelle, D. J., and Agarwal, U. P. 2016. Techniques for characterizing lignin. Pages 49-66 in: Lignin in Polymer Composites. O. Faruk and M. Sain, eds. Elsevier, Amsterdam, the Netherlands.
Stegmann, M., Monaghan, J., Smakowska-Luzan, E., Rovenich, H., Lehner, A., Holton, N., Belkhadir, Y., and Zipfel, C. 2017. The receptor kinase FER is a RALF-regulated scaffold controlling plant immune signaling. Science 355:287-289.
Swaminathan, S., Lionetti, V., and Zabotine, O. A. 2022. Plant cell wall integrity perturbations and priming for defense. Plants 11:3539.
Thaler, J. S., Owen, B., and Higgins, V. J. 2004. The role of the jasmonate response in plant susceptibility to diverse pathogens with a range of lifestyles. Plant Physiol. 135:530-538.
Turner, S. R., and Somerville, C. R. 1997. Collapsed xylem phenotype of Arabidopsis identifies mutants deficient in cellulose deposition in the secondary cell wall. Plant Cell 9:689-701.
Underwood, W., and Somerville, S. C. 2008. Focal accumulation of defences at sites of fungal pathogen attack. J. Exp. Bot. 59:3501-3508.
Vaahtera, L., Schulz, J., and Hamann, T. 2019. Cell wall integrity maintenance during plant development and interaction with the environment. Nat. Plants 5:924-932.
Wei, Z., Huang, J.-F., Hu, J., Gu, Y.-A., Yang, C.-L., Mei, X.-L., Shen, Q.-R., Xu, Y.-C., and Friman, V.-P. 2015. Altering transplantation time to avoid periods of high temperature can efficiently reduce bacterial wilt disease incidence with tomato. PLoS One 10:e0139313.
Williamson, R. E., Burn, J. E., Birch, R., Baskin, T. I., Arioli, T., Betzner, A. S., and Cork, A. 2001. Morphology of *rsw1*, a cellulose-deficient mutant of *Arabidopsis thaliana*. Protoplasma 215:116-127.
Wolf, S., Hématy, K., and Höfte, H. 2012. Growth control and cell wall signaling in plants. Annu. Rev. Plant Biol. 63:381-407.